Comput. Methods Appl. Mech. Engrg. 199 (2010) 961–978

Contents lists available at ScienceDirect

Comput. Methods Appl. Mech. Engrg.

journal homepage: www.elsevier.com/locate/cma

Error assessment and mesh adaptivity for regularized continuous failure models

T. Pannachet [a,*], P. Díez [b], H. Askes [c], L.J. Sluys [d]

[a] Khon Kaen University, Faculty of Engineering, Ampor Muang, Khon Kaen 40002, Thailand
[b] Universitat Politècnica de Catalunya, Departament de Matemàtica Aplicada III, Jordi Girona 1–3, E-08034 Barcelona, Spain
[c] University of Sheffield, Department of Civil and Structural Engineering, Mappin Street, S1 3JD Sheffield, UK
[d] Delft University of Technology, Faculty of Civil Engineering and Geosciences, P.O. Box 5048, 2600 GA Delft, The Netherlands

ARTICLE INFO

Article history:
Received 26 March 2009
Received in revised form 21 September 2009
Accepted 10 November 2009
Available online 26 November 2009

Keywords:
Gradient-enhanced damage model
Error estimation
Quantity of interest
Goal-oriented error estimation

ABSTRACT

This paper deals with the adaptive finite element analysis of structural failure. A gradient-enhanced damage model has been chosen to simulate material degradation. Since this model is regularized in the post-peak regime, the finite element solution does not suffer from pathological mesh dependence and thus converges to an objective solution upon mesh refinement. However, the error analyses have shown that the error in the nonlocal equivalent strain field becomes dominant during the post-peak loading stages. The accuracy of the nonlocal equivalent strain field (and the corresponding damage quantity) also greatly influences the accuracy of the quantity of interest. Two error measures have been proposed. The goal-oriented error estimates have provided similar error distributions, although some small differences have been found in the softening regime. Objective error estimates, together with adaptive criteria, have been used to perform automated *h*-adaptivity during computation.

1. Introduction

Quasi-brittle materials such as plain concrete exhibit so-called *strain softening behavior*. Once damage is initiated, these materials are still able to carry some residual load while gradually losing their strength. During such processes, deformation tends to concentrate in some parts of the material, subsequently forming cracks which finally leads to failure.

The phenomenon can suitably be modelled by means of *damage mechanics*. The formation and growth of a microstructural crack is modelled via continuous damage variables, such that failure can be simulated entirely within a continuum mechanics framework. During damage growth, the material gradually loses its integrity and its stored energy is dissipated. Unfortunately, a straightforward inclusion of a damage-driven dissipation results in mathematical ill-posedness in the post-peak regime of the structural response, causing a zero width of the localization zone and subsequently zero energy dissipation. As a result, the finite element size controls the localization width, leading to so-called *mesh dependence* [29] in the sense that the numerical results do not converge when the discretization is refined in finite element modelling. Error estimation and adaptivity would consequently not give meaningful results. Information on microscopic material behavior must be taken into account in the continuum model. This can be achieved by enhancing the continuum model with an intrinsic length scale to avoid the loss of ellipticity. As a regularized model, the implicit gradient-enhanced damage model [27] is chosen for this study.

Even though the numerical results converge upon refinement of discretization, the finite element modelling requires an adequate mesh discretization in order to accurately describe the fracture processes. A way to consider whether the discretization used in the analysis is sufficient, meaning the results are acceptably accurate, is to measure the *discretization error*. Error estimation, as well as error indication, has been applied in problems with softening phenomena. Error indication does not provide objective information about the exact error, but gives some hints as to where the solution may need a more refined/enriched discretization. It relies on heuristic observations – for example, errors tend to concentrate in the strain localization zone during damage evolution [3,41]. However, to choose an efficient error indicator, there should be some objective links between the indicating variables and the actual discretization error. To this end, objective error estimation can play an important role.

Residual-type error estimation has been applied to softening media such as viscoplastic or nonlocal damage models [11,34]. In these works, the error estimation takes place only at the end of the analysis. As a result, the information on how the error *evolves* during the computation is lost. However, it has been reported [9] that the error estimate (for example, [18]) may become less significant in the localization region as damage grows and stresses tend to vanish.

In this contribution, the error estimator presented in [25] is extended to nonlinear finite element analysis. Pioneered by Díez et al. [12], the scheme is based on solving a series of local problems,

* Corresponding author. Tel.: +66 85 0033343; fax: +66 43 202846.
E-mail address: tanpan@kku.ac.th (T. Pannachet).

0045-7825/$ - see front matter © 2009 Elsevier B.V. All rights reserved.
doi:10.1016/j.cma.2009.11.010

based on patches consisting of elements surrounding each node, with prescribed homogeneous essential boundary conditions. In Section 3, we will show how the nonlinear problem (cf. Section 2) is brought to a linearized error equation. In this framework, the evolution of the discretization error can be obtained by applying error estimation during computation. To assess the error in certain quantities of interest, we investigate two goal-oriented error estimates which are formulated in a positive-definite norm setting (cf. Section 4). In addition, uniform mesh discretizations of varying resolutions and polynomial orders are surveyed, as a preliminary study to adaptive discretization presented at the end of each numerical example.

2. The gradient-enhanced damage model

In this research, the gradient-enhanced damage model [27,40] is chosen. As a regularized continuum, the gradient-enhanced damage model converges properly upon refinement of the finite element discretization.

Let Ω be a bounded domain with the boundary $\partial\Omega$. The boundary consists of the Dirichlet boundary Γ_d and the Neumann boundary Γ_n for which $\Gamma_d \cap \Gamma_n = \emptyset$ and $\overline{\Gamma_d \cup \Gamma_n} = \partial\Omega$. In the standard finite element analysis, for a problem in statics, we try to find the unknown solution $\boldsymbol{u}$ of the variational boundary value problem

$$\int_\Omega \boldsymbol{\varepsilon}(\boldsymbol{v}) : \boldsymbol{\sigma}(\boldsymbol{u})\ \mathrm{d}\Omega = \int_{\Gamma_n} \boldsymbol{v}\cdot\boldsymbol{g}\ \mathrm{d}\Gamma + \int_\Omega \boldsymbol{v}\cdot\boldsymbol{q}\ \mathrm{d}\Omega, \tag{1}$$

which can be written in terms of derivatives of trial and test functions, $\boldsymbol{u}$ and $\boldsymbol{v}$, as

$$\int_\Omega (\nabla\boldsymbol{v}) : \boldsymbol{D} : (\nabla\boldsymbol{u})\ \mathrm{d}\Omega = \int_{\Gamma_n} \boldsymbol{v}\cdot\boldsymbol{g}\ \mathrm{d}\Gamma + \int_\Omega \boldsymbol{v}\cdot\boldsymbol{q}\ \mathrm{d}\Omega. \tag{2}$$

The test function $\boldsymbol{v}$ is any arbitrary function in the Sobolev space $\mathscr{V}$, which is defined by $\mathscr{V} := \{\boldsymbol{v} \in (H^1(\Omega))^d; \boldsymbol{v} = 0 \text{ on } \Gamma_d\}$, with the geometrical dimension d. Moreover, $\boldsymbol{\varepsilon}(\boldsymbol{v}) := \nabla\boldsymbol{v}$ and $\boldsymbol{\sigma}(\boldsymbol{u}) := \boldsymbol{D} : \nabla\boldsymbol{u}$ represent strains and stresses, $\boldsymbol{g}$ represents the traction forces along the boundary Γ_n and $\boldsymbol{q}$ denotes the body forces in the domain Ω.

Within the context of continuum damage mechanics, material gradually loses its load-carrying capacity as a result of the appearance of microstructural cracks. This material degradation process, described here in a continuum damage mechanics concept by the introduction of a scalar damage parameter ω, is cast in a stress–strain relation as

$$\boldsymbol{\sigma} = (1-\omega)\boldsymbol{D}^e : \boldsymbol{\varepsilon}, \tag{3}$$

where $\boldsymbol{\sigma}$ and $\boldsymbol{\varepsilon}$ denote stresses and strains and $\boldsymbol{D}^e$ is the linear-elastic constitutive tensor. The damage parameter ω ranges from 0 (for virgin condition) to 1 (for fully damaged condition) and is defined as a function of a history parameter κ, i.e. $\omega := \omega(\kappa)$.

Representing the largest value of the deformation in the loading history, κ is obtained from

$$\kappa = \max\ (\kappa_0, \varepsilon_{\mathrm{eq}}), \tag{4}$$

where κ_0 is a user-specified damage threshold and $\varepsilon_{\mathrm{eq}}$ refers to an equivalent strain, which is a scalar invariant representing the strains. Some definitions of this equivalent strain are, for example,

- *Mazars definition* [22]

$$\varepsilon_{\mathrm{eq}} = \sqrt{\sum_{i=1}^{3} \langle\varepsilon_i\rangle^2}, \tag{5}$$

where ε_i denotes the principal strain and the positive principal strain $\langle\varepsilon_i\rangle$ is defined as

$$\langle\varepsilon_i\rangle = \frac{\varepsilon_i + |\varepsilon_i|}{2}. \tag{6}$$

- *Modified von Mises definition* [10]

$$\varepsilon_{\mathrm{eq}} = \frac{k-1}{2k(1-2\nu)} I_1 + \frac{1}{2k}\sqrt{\frac{(k-1)^2}{(1-2\nu)^2} I_1^2 + \frac{12k}{(1+\nu)^2} J_2}, \tag{7}$$

where k is the ratio of the compressive and tensile strength, and the strain invariants I_1 and J_2 are defined as

$$I_1 = \varepsilon_{xx} + \varepsilon_{yy} + \varepsilon_{zz}, \tag{8}$$

$$J_2 = \frac{(\varepsilon_{xx}^2 + \varepsilon_{yy}^2 + \varepsilon_{zz}^2 - \varepsilon_{xx}\varepsilon_{yy} - \varepsilon_{yy}\varepsilon_{zz} - \varepsilon_{zz}\varepsilon_{xx})}{3} + \varepsilon_{xy}^2 + \varepsilon_{yz}^2 + \varepsilon_{zx}^2. \tag{9}$$

Damage evolves when the Kuhn–Tucker conditions

$$f \leqslant 0, \quad \dot{\kappa} \geqslant 0, \quad \dot{\kappa} f = 0, \tag{10}$$

are satisfied. The loading function f is defined as

$$f = \varepsilon_{\mathrm{eq}} - \kappa. \tag{11}$$

Damage growth is described by means of softening laws. An example of such laws is the *exponential softening law* [28]

$$\omega = 1 - \frac{\kappa_0}{\kappa}(1 - \alpha + \alpha\ \exp\ (-\beta(\kappa - \kappa_0))) \quad \text{if } \kappa \geqslant \kappa_0, \tag{12}$$

where α and β are material parameters controlling the residual stress and the damage growth rate, respectively.

The above formulation is a standard local damage model. As mentioned above, due to a lack of microstructural information, the localization zone tends to have a zero width. The above model suffers from mathematical ill-posedness and, consequently, a severe mesh dependence [29]. To overcome these problems, some techniques have been introduced. In this study, we employ regularization based on replacing the local equivalent strain $\varepsilon_{\mathrm{eq}}$ by the nonlocal equivalent strain $\breve{\varepsilon}_{\mathrm{eq}}$ in Eqs. (4) and (11).

By averaging the local equivalent strain in the gradient form, the nonlocal equivalent strain can be defined in an implicit gradient enhancement form of [27]

$$\breve{\varepsilon}_{\mathrm{eq}} - c\nabla^2\breve{\varepsilon}_{\mathrm{eq}} = \varepsilon_{\mathrm{eq}}, \tag{13}$$

where c is a material parameter based on the intrinsic length scale l_{int} and is defined as

$$c = \frac{1}{2} l_{\mathrm{int}}^2. \tag{14}$$

The intrinsic length scale has the dimension of length and it is a representation of the underlying microstructure of the material. Inclusion of an internal length scale as done in Eq. (13) ensures that the failure zone has a finite width, which in turn guarantees a non-zero energy dissipation upon mesh refinement. Thus, the problems of the local damage model are overcome [27,28].

Applying integration by parts, the implicit gradient enhancement formulation [27] can be cast in a weak form as

$$\int_\Omega \delta\breve{\varepsilon}_{\mathrm{eq}}\breve{\varepsilon}_{\mathrm{eq}}\ \mathrm{d}\Omega + \int_\Omega \nabla\delta\breve{\varepsilon}_{\mathrm{eq}} c \nabla\breve{\varepsilon}_{\mathrm{eq}}\ \mathrm{d}\Omega = \int_\Omega \delta\breve{\varepsilon}_{\mathrm{eq}}\varepsilon_{\mathrm{eq}}\ \mathrm{d}\Omega, \quad \forall\delta\breve{\varepsilon}_{\mathrm{eq}} \in (H^1(\Omega))^d. \tag{15}$$

Note that to improve the conditioning of the stiffness matrix given in Eq. (20), the use of the Young's modulus E as a scaling factor for both sides of Eq. (15) may be considered.

Combining Eqs. (2) and (15), the Galerkin weak form can be written as

$$\mathscr{B}(\breve{\boldsymbol{u}}, \boldsymbol{v}) = \mathscr{F}(\boldsymbol{v}), \quad \forall\boldsymbol{v} \in \mathscr{V}, \tag{16}$$

where $\breve{\boldsymbol{u}} = \{\boldsymbol{u}, \breve{\varepsilon}_{\mathrm{eq}}\}$ and the term $\mathscr{B}(\cdot,\cdot)$ is a symmetric positive-definite bilinear form.

3. Error analysis

We have chosen a residual-type error estimator, introduced in [25], in this study. Using this method, we solve a series of local problems based on a patch of elements, which are enriched by one order higher interpolation, with prescribed homogeneous boundary conditions. The method is applied for estimating the error in energy norm, as well as the error in a local quantity of interest (cf. Section 4). Note that the so-called guaranteed bounds on the error is not considered in this paper. The gradient-enhanced damage model formulated in the last section includes two sets of unknowns, namely the displacement field and the nonlocal equivalent strain field. For the second-order implicit gradient formulation, cf. Eq. (13), $\mathscr{C}^0$ shape functions are required. The discrete approximation to $\breve{\boldsymbol{u}}$ is denoted $\breve{\boldsymbol{u}}_{(h,p)}$ where h stands for the characteristic element size and p for the degree of the interpolation in the elements of the mesh. The set of unknowns is the solution of the system of equations

$$\mathscr{B}^{\text{tang}}(\Delta\breve{\boldsymbol{u}}_{(h,p)}, \boldsymbol{v}_{(h,p)})|_{(t-1:\ t)} = \Delta\mathscr{F}(\boldsymbol{v}_{(h,p)})|_{(t-1:\ t)}, \tag{17}$$

where the bilinear form $\mathscr{B}^{\text{tang}}(\cdot,\cdot)$, using a tangent representation, is a linearized form of $\mathscr{B}(\cdot,\cdot)$ defined on $\mathscr{V}\times\mathscr{V}\to R$. The term $\Delta\mathscr{F}(\cdot)$ represents a stepwise force vector defined on $\mathscr{V}\to R$. The test function $\boldsymbol{v}$ is any arbitrary function in the Sobolev space $\mathscr{V}$, which is defined by $\mathscr{V} := \{\boldsymbol{v}\in(H^1(\Omega))^d; \boldsymbol{v}=0 \text{ on } \Gamma_d\}$.

By applying a series of proportional loadings, the solution $\breve{\boldsymbol{u}}$ is updated during the Newton–Raphson iterative scheme, i.e.

$$\breve{\boldsymbol{u}}_{(h,p)}|_{(t)} = \breve{\boldsymbol{u}}_{(h,p)}|_{(t-1)} + \Delta\breve{\boldsymbol{u}}_{(h,p)}|_{(t-1:\ t)}. \tag{18}$$

Here, the subscript (t) denotes a computational time step and $(t-1:t)$ presents a measure between the previous time step $(t-1)$ and the present time step (t). It is natural to include all unknown degrees of freedom existing in the formulation in the error analysis, as all of them are primary unknowns in the finite element computation. The error $\breve{\boldsymbol{e}} := \breve{\boldsymbol{u}} - \breve{\boldsymbol{u}}_{(h,p)}$ is for all practical purposes replaced by a reference error associated with a finer discretization $(\tilde{h},\tilde{p})$ (with either $\tilde{h}<h$ or $\tilde{p}>p$), namely $\breve{\boldsymbol{e}}_{(\tilde{h},\tilde{p})} := \breve{\boldsymbol{u}}_{(\tilde{h},\tilde{p})} - \breve{\boldsymbol{u}}_{(h,p)}$. The reference error is determined solving a residual linearized problem

$$\mathscr{B}^{\text{tang}}(\breve{\boldsymbol{e}}_{(\tilde{h},\tilde{p})}, \boldsymbol{v})|_{(t)} = \mathscr{R}^{\breve{u}}(\boldsymbol{v}_{(\tilde{h},\tilde{p})})|_{(t)} = \mathscr{F}(\boldsymbol{v}_{(\tilde{h},\tilde{p})})|_{(t)} - \mathscr{B}(\breve{\boldsymbol{u}}_{(h,p)}, \boldsymbol{v}_{(\tilde{h},\tilde{p})})|_{(t)}, \tag{19}$$

for every test function in $\breve{\boldsymbol{v}}_{(\tilde{h},\tilde{p})}$ in the test space associated with the fine $(\tilde{h},\tilde{p})$ discretization, $\mathscr{V}$. The term $\mathscr{R}^{u}(\boldsymbol{v}_{(\tilde{h},\tilde{p})})|_{(t)}$ denotes the discretization residuals measured using the reference mesh $(\tilde{h},\tilde{p})$ at computational time t. In the following, for the sake of a simpler presentation, the subscript $(\tilde{h},\tilde{p})$ is suppressed in the notation for the reference error because the *exact* error is no longer considered.

The error computation follows the process described in [25], whereby a series of patch-based computations is solved instead of a global computation. The finite element discretization leads to a consistent tangent stiffness matrix of the form

$$\boldsymbol{K} = \mathscr{B}^{\text{tang}}(\breve{\boldsymbol{\phi}},\breve{\boldsymbol{\phi}}) = \begin{bmatrix} \boldsymbol{K}_{uu} & \boldsymbol{K}_{u\breve{\varepsilon}} \\ \boldsymbol{K}_{\breve{\varepsilon}u} & \boldsymbol{K}_{\breve{\varepsilon}\breve{\varepsilon}} \end{bmatrix}, \tag{20}$$

with

$$\boldsymbol{K}_{uu} = \int_\Omega \nabla\boldsymbol{\phi}_u :\ (1-\omega)\boldsymbol{D}^e :\ \nabla\boldsymbol{\phi}_u \,\mathrm{d}\Omega, \tag{21}$$

$$\boldsymbol{K}_{u\breve{\varepsilon}} = -\int_\Omega \nabla\boldsymbol{\phi}_u :\ \boldsymbol{s}_{u\breve{\varepsilon}} :\ \boldsymbol{\phi}_{\breve{\varepsilon}} \,\mathrm{d}\Omega, \tag{22}$$

$$\boldsymbol{K}_{\breve{\varepsilon}u} = -\int_\Omega \boldsymbol{\phi}_{\breve{\varepsilon}} :\ \boldsymbol{s}_{\breve{\varepsilon}u} :\ \nabla\boldsymbol{\phi}_u \,\mathrm{d}\Omega, \tag{23}$$

$$\boldsymbol{K}_{\breve{\varepsilon}\breve{\varepsilon}} = \int_\Omega (\boldsymbol{\phi}_{\breve{\varepsilon}}\cdot\boldsymbol{\phi}_{\breve{\varepsilon}} + \nabla\boldsymbol{\phi}_{\breve{\varepsilon}} :\ c\nabla\boldsymbol{\phi}_{\breve{\varepsilon}}) \,\mathrm{d}\Omega, \tag{24}$$

and

$$\boldsymbol{s}_{\breve{\varepsilon}u} = \frac{\partial\varepsilon_{\text{eq}}}{\partial\boldsymbol{\varepsilon}} \text{ and } \boldsymbol{s}_{u\breve{\varepsilon}} = \frac{\partial\omega}{\partial\breve{\varepsilon}}\boldsymbol{D}^e\boldsymbol{\varepsilon}. \tag{25}$$

It should be noted that $\boldsymbol{\phi}$ are shape functions corresponding to the fine $(\tilde{h},\tilde{p})$ discretization. Quadratic shape functions $\boldsymbol{\phi}_u$ and linear shape functions $\boldsymbol{\phi}_{\breve{\varepsilon}}$ are used for the two sets of unknowns, although they may be chosen from the same space [40]. For a discussion on the finite element implementation of the model, the reader is referred to [39,40].

By using a softening model, it is possible that the computation of the error norm via the use of the consistent tangent stiffness matrix $\boldsymbol{K}$ leads to a negative value and thus the energy norm, usually defined as

$$(\|\breve{\boldsymbol{u}}\|)^2 = \mathscr{B}^{\text{tang}}(\breve{\boldsymbol{u}},\breve{\boldsymbol{u}}) = \breve{\boldsymbol{u}} :\ \boldsymbol{K} :\ \breve{\boldsymbol{u}}, \tag{26}$$

becomes meaningless. To avoid such problems, we employ here only those parts of the stiffness matrix which include $\boldsymbol{K}_{uu}$ and $\boldsymbol{K}_{\breve{\varepsilon}\breve{\varepsilon}}$. It can be seen from the discretized equations that the terms $\boldsymbol{K}_{u\breve{\varepsilon}}$ and $\boldsymbol{K}_{\breve{\varepsilon}u}$ may lead to non-positive-definite contributions to the global stiffness matrix. On the other hand, $\boldsymbol{K}_{uu}$ and $\boldsymbol{K}_{\breve{\varepsilon}\breve{\varepsilon}}$ remain positive-definite in the whole loading process. To maintain a mathematically meaningful norm for the error, the interaction between the two sets of degrees of freedom (i.e. $\boldsymbol{u}$ and $\breve{\varepsilon}_{\text{eq}}$) is neglected, thus avoiding the occurrence of a negative-definite matrix in the error norm computation. The modified stiffness matrix for the norm computation reads

$$\boldsymbol{K}^+ = \mathscr{B}^{\text{tang}+}(\breve{\boldsymbol{\phi}},\breve{\boldsymbol{\phi}}) = \begin{bmatrix} \boldsymbol{K}_{uu} & \boldsymbol{0} \\ \boldsymbol{0} & \boldsymbol{K}_{\breve{\varepsilon}\breve{\varepsilon}} \end{bmatrix}. \tag{27}$$

Note that $\boldsymbol{K}_{uu}$ is also the *secant stiffness matrix*, cf. Eq. (21). The energy norm of the solution and the error can then be written, respectively, as

$$\begin{aligned}(\|\breve{\boldsymbol{u}}\|^+)^2 &= \mathscr{B}^{\text{tang}+}(\breve{\boldsymbol{u}},\breve{\boldsymbol{u}}) = (\|\boldsymbol{u}\|^+)^2 + (\|\breve{\boldsymbol{\varepsilon}}_{\text{eq}}\|^+)^2 \\ &= \boldsymbol{u} :\ \boldsymbol{K}_{uu} :\ \boldsymbol{u} + \breve{\boldsymbol{\varepsilon}}_{\text{eq}} :\ \boldsymbol{K}_{\breve{\varepsilon}\breve{\varepsilon}} :\ \breve{\boldsymbol{\varepsilon}}_{\text{eq}},\end{aligned} \tag{28}$$

$$\begin{aligned}(\|\breve{\boldsymbol{e}}\|^+)^2 &= \mathscr{B}^{\text{tang}+}(\breve{\boldsymbol{e}},\breve{\boldsymbol{e}}) = (\|\boldsymbol{e}_u\|^+)^2 + (\|\boldsymbol{e}_{\breve{\varepsilon}}\|^+)^2 \\ &= \boldsymbol{e}_u :\ \boldsymbol{K}_{uu} :\ \boldsymbol{e}_u + \boldsymbol{e}_{\breve{\varepsilon}} :\ \boldsymbol{K}_{\breve{\varepsilon}\breve{\varepsilon}} :\ \boldsymbol{e}_{\breve{\varepsilon}}.\end{aligned} \tag{29}$$

Note that, since a tangential form $\mathscr{B}^{\text{tang}}(\cdot,\cdot)$ will always be used in the nonlinear settings from this point on, the superscript tang will be dropped for simplicity.

4. Goal-oriented error estimation

Although the error measured in the energy norm gives a good indication of the overall error, it may also be relatively insensitive to certain local values of the state variables and their accuracy. In other words, a small error in energy norm does not always guarantee that the local quantities of interest, such as stresses or damage profile in a critical region, are sufficiently accurate. For the problems where there are some specific goals in mind, estimation of error of these specific quantities can provide more relevant information for the adaptive finite element process.

The error can be measured with respect to a specific goal via the framework of *goal-oriented error estimation*. Some pioneering works on this subject include [4,31,7] for problems in linear elasticity, which have also been further extended to various problems such as plasticity [32,33,8], viscoelasticity [6] and crack problems [36,16,15]. In addition, there have been some efforts in getting bounds on the error [30,23,37].

In this study, we also estimate the error in chosen quantities of interest in any local domain. At some extra cost, the goal-oriented error estimation can be set and applied at the end of

any computational step in the finite element analysis. Techniques for goal-oriented error measurement make use of the concept of an *influence function*, which in the context of error estimation indicates how the discretization error affects the specific quantity of interest. That is, to measure such an error quantity, an additional boundary value problem needs to be solved. This so-called *dual (adjoint) problem* is constructed in a dual argument setting and makes use of Maxwell's *reciprocal theorem*. Once the dual problem is solved, the discretization residuals can be redistributed according to the influence function to provide a proper error measure to the selected goal quantity.

4.1. Setting of error in the goal quantity

The most crucial point of the goal-oriented error measurement is how to choose the quantity of interest $Q(\boldsymbol{u})$ such that it can be analysed straightforwardly. Basically, the choice depends on the model problem to be analysed and may be chosen in the forms of domain integrals [15], contour integrals [36,16] or pointwise quantities [30,1]. Ideally, $Q(u)$ is a linear functional; if not, one of the linearization techniques [37,19,35] should be applied.

Considering the quantity of interest $Q(\boldsymbol{u})$, we can define the discretization error of this quantity as

$$\mathscr{E} := Q(\boldsymbol{u}) - Q(\boldsymbol{u}_{(h,p)}). \tag{30}$$

Here, we restrict ourselves to the case in which $Q(\boldsymbol{u})$ is a linear functional and, consequently, the error of the goal-oriented quantity can be rewritten as

$$\mathscr{E} = Q(\boldsymbol{u}) - Q(\boldsymbol{u}_{(h,p)}) = Q(\boldsymbol{u} - \boldsymbol{u}_{(h,p)}) = Q(\boldsymbol{e}), \tag{31}$$

where $Q(\boldsymbol{e})$ denotes the discretization error of the finite element analysis (primal problem) measured in the quantity of interest. The dual (or adjoint) problem is introduced as

$$\mathscr{B}(\boldsymbol{v}, \boldsymbol{w}) = Q(\boldsymbol{v}) \qquad \forall \boldsymbol{v} \in \mathscr{V}, \tag{32}$$

to find the solution $\boldsymbol{w} \in \mathscr{V}$. Note that once the influence function $\boldsymbol{w}$ is known, $Q(\boldsymbol{e})$ is recovered as

$$Q(\boldsymbol{e}) = \mathscr{B}(\boldsymbol{e}, \boldsymbol{w}) = R^{\ddot{u}}(\boldsymbol{w}), \tag{33}$$

which implies that the influence function acts as a weight function for distribution of the discretization error $\boldsymbol{e}$ to the quantity Q in an energy norm measure. This expression is the so-called error representation which can be rewritten in terms of the error of the solution of the dual problem, $\epsilon := \boldsymbol{w} - \boldsymbol{w}_{(h,p)}$ (which is in practice replaced by the reference counterpart $\epsilon := \boldsymbol{w}_{(\hat{h},\hat{p})} - \boldsymbol{w}_{(h,p)}$ as for the direct problem (Eq. 17)). In fact,

$$Q(\boldsymbol{e}) = B(\boldsymbol{e}, \boldsymbol{w}_{(h,p)} + \epsilon) = B(\boldsymbol{e}, \boldsymbol{w}_{(h,p)}) + B(\boldsymbol{e}, \epsilon) = B(\boldsymbol{e}, \epsilon). \tag{34}$$

Note that the term $B(\boldsymbol{e}, \boldsymbol{w}_{(h,p)})$ vanishes because Galerkin orthogonality holds in the solution of the primal problem.

In nonlinear finite element analysis, the Newton–Raphson iterative procedure is generally applied to obtain the solution of the physical (primal) problem. This incremental loading procedure is, however, not needed in the dual framework, as the solution of the dual problem indicates the influence of the primal solution at a loading step to the quantity of interest. In other words, a linear solution control should be sufficient for analysing the dual problem.

During the nonlinear (primal) solution control, a set of discretized dual equations may be set based on the tangent representation at the time of computation. Following the linear-elastic case, error analysis in the dual framework is then straightforwardly carried out by means of the error equation

$$\mathscr{B}(\boldsymbol{v}, \epsilon) = \mathscr{R}^{w}(\boldsymbol{v}) = Q(\boldsymbol{v}) - \mathscr{B}(\boldsymbol{v}, \boldsymbol{w}_{(h,p)}), \tag{35}$$

by which the error from solving the dual problem ϵ can be estimated. The error is computed based on patches of elements and the computational procedure follows the same procedure as described in [25].

Fig. 1 shows the procedure in the goal-oriented error estimation. Two global sets of equations, namely the primal and the dual problems, are solved. However, one can utilize the factorized global stiffness matrix, which is formed during the solving of the primal problem, also in the dual problem. This factorization, in fact, is the main computation in solving the global equations. Thus, backsubstitution to the factorized matrix to obtain the solution of the dual problem can save considerable computational time.

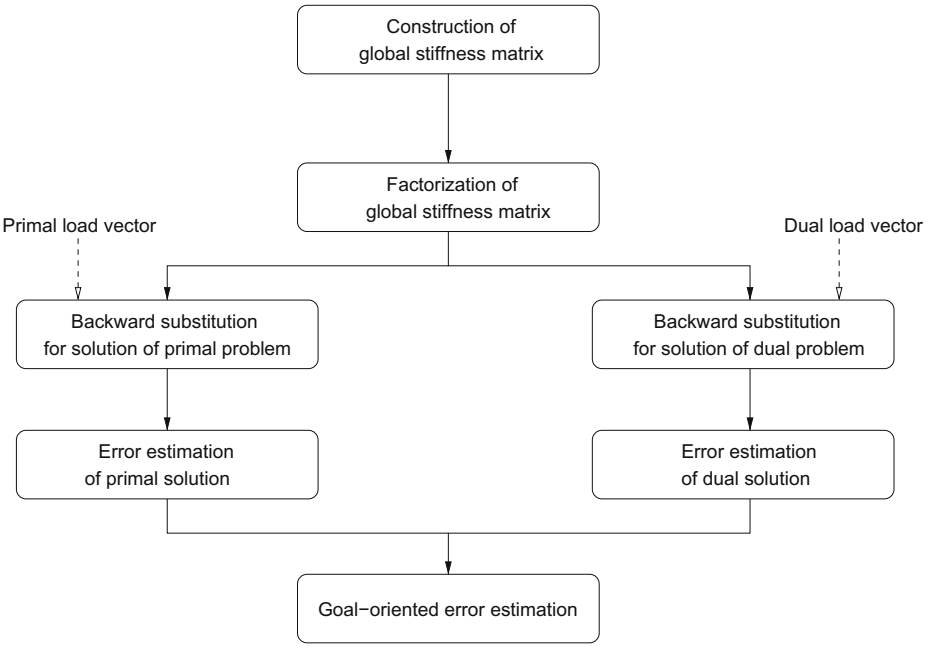

Fig. 1. Goal-oriented error estimation procedure.

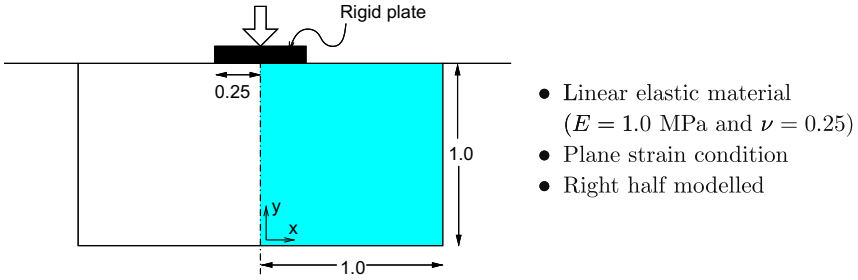

Fig. 2. Prandtl's punch test. Dimensions are in mm.

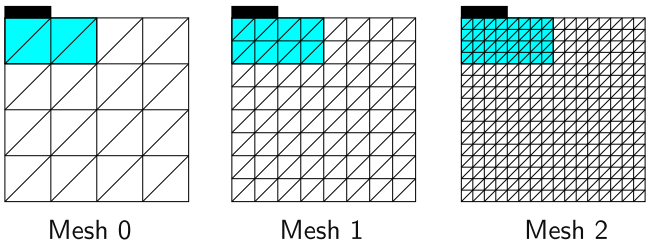

Fig. 3. Finite element meshes used in the computation. The shaded area is the area of interest Ω_s.

4.2. Choices of error measures in local domains

The finite element mesh (h, p) is composed by elements Ω_k, $k = 1, 2, \ldots$ covering the whole domain Ω. The restriction of the bilinear form $B(\cdot,\cdot)$ to Ω_k is denoted by $B_k(\cdot,\cdot)$. Accordingly, the globally defined error quantity $Q(\boldsymbol{e})$ is split into elemental contributions as

$$Q(\boldsymbol{e}) = \sum_k Q_k, \tag{36}$$

where

$$Q_k = \mathscr{B}_k(\boldsymbol{e}, \boldsymbol{w}_{(h,p)}) + \mathscr{B}_k(\boldsymbol{e}, \epsilon). \tag{37}$$

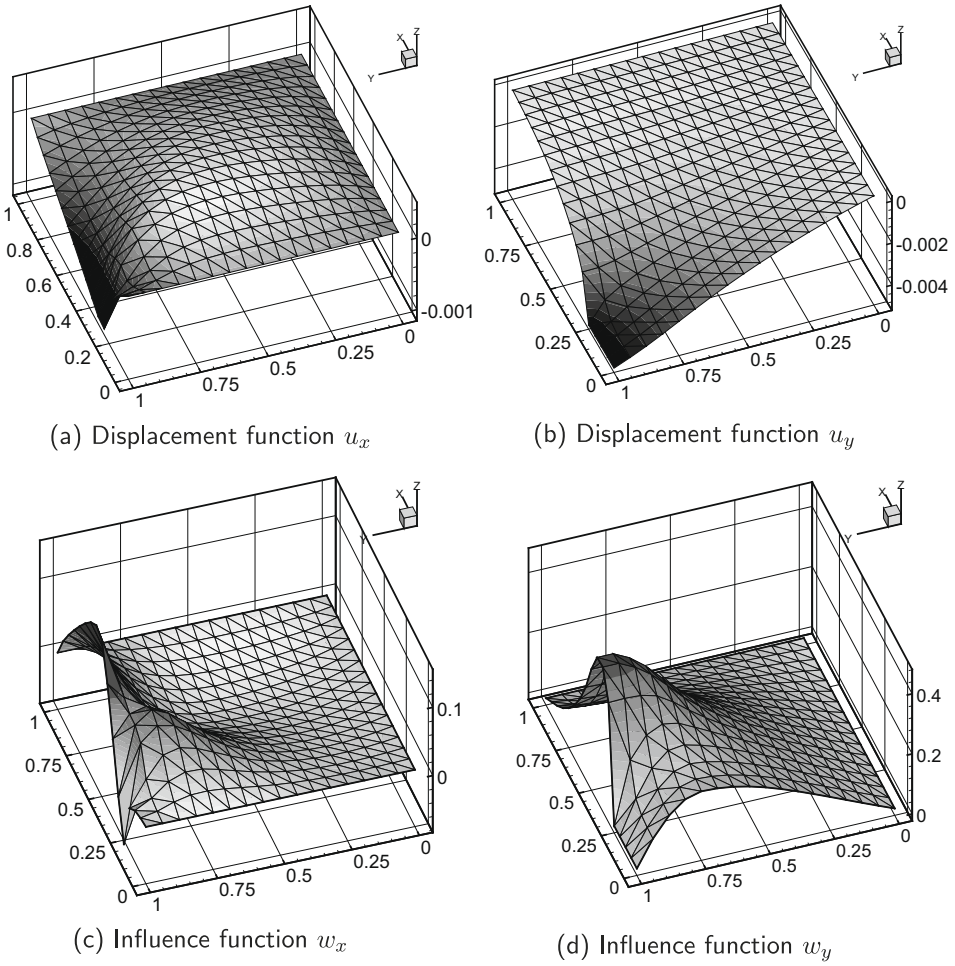

Fig. 4. The displacement function and the influence functions, obtained using the reference mesh, i.e. Mesh 2 with the quartic interpolation ($p = 4$).

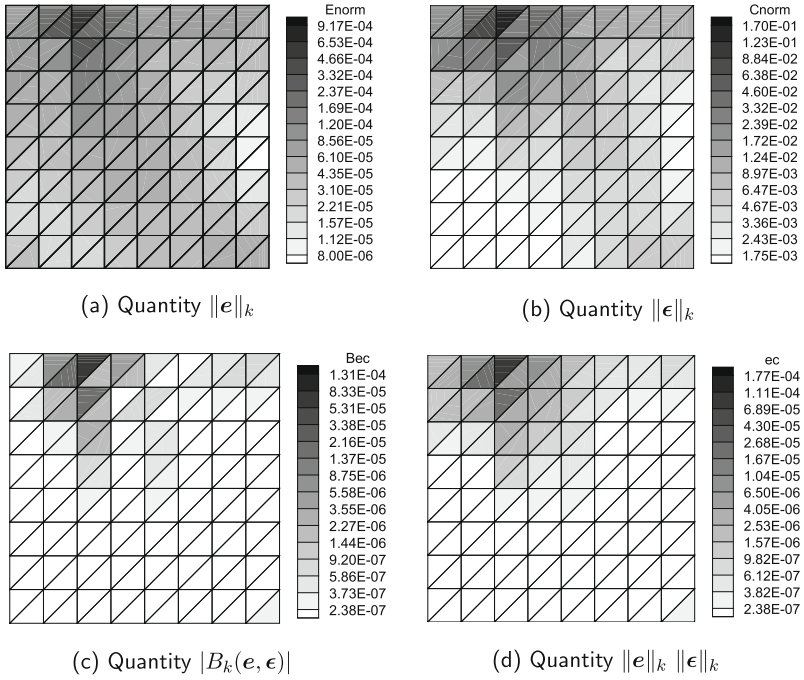

(a) Quantity $\|\boldsymbol{e}\|_k$ (b) Quantity $\|\boldsymbol{\epsilon}\|_k$

(c) Quantity $|B_k(\boldsymbol{e},\boldsymbol{\epsilon})|$ (d) Quantity $\|\boldsymbol{e}\|_k\ \|\boldsymbol{\epsilon}\|_k$

Fig. 5. Distribution of the elemental error measures in the framework of primal and dual problem, as well as the goal-oriented framework. The linear interpolation in Mesh 1 is employed. Exponential scaling is used.

It should be noted that the first right-hand-side term of Eq. (37) does not necessarily cancel since Galerkin's orthogonality property does not hold in this local setting. Nevertheless, it has been proven that the second term can represent the distribution of the error in the local region effectively [14].

To simplify the adaptive criteria, the absolute value of the term is employed. We have chosen the first measure as

$$\mathscr{E}_k^I := |\mathscr{B}_k(\boldsymbol{e},\boldsymbol{\epsilon})|, \tag{38}$$

which is chosen as our first alternative for representing the error in the elemental region Ω_k.

For positive-definite stiffness matrices, the second alternative is related to the first one by the Cauchy–Schwarz's inequality, i.e.

$$|\mathscr{B}_k(\boldsymbol{e},\boldsymbol{\epsilon})| \leqslant \|\boldsymbol{e}\|_k\|\boldsymbol{\epsilon}\|_k, \tag{39}$$

leading to the local error measure [1,14]

$$\mathscr{E}_k^{II} := \|\boldsymbol{e}\|_k\|\boldsymbol{\epsilon}\|_k. \tag{40}$$

Replacing the use of Eq. (36), two corresponding global indicators may be set by summing up the local indicators as

$$\mathscr{E}^I = \sum_k \mathscr{E}_k^I, \tag{41}$$

and

$$\mathscr{E}^{II} = \sum_k \mathscr{E}_k^{II}. \tag{42}$$

These two estimates provide a straightforward formulation of the adaptive and optimality criteria (to be mentioned in Section 5) as the global measures are computed by directly summing up the local measures.

4.3. Illustration: punch problem

Performances of the goal-oriented error measures are investigated in Prandtl's punch test. A rigid plate is pushed into a confined linear elastic material. The detailed description of the model problem is given in Fig. 2. Three selected meshes, shown in Fig. 3, are used in this finite element analysis.

For this problem, we choose our goal quantity to be

$$Q(\boldsymbol{u}) = \int_{\Omega_s} u_y(\boldsymbol{x})\ d\Omega, \tag{43}$$

where $u_y(\boldsymbol{x})$ denotes the displacement in the y-direction at any point $\boldsymbol{x}$, and the area of interest Ω_s is defined as the shaded area in Fig. 3. The solutions of the primal problem, as well as those of the dual problem, are plotted in Fig. 4.

Considering the elemental distribution of the estimated error in the quantity of interest shown in Figs. 5 and 6, it is observed that both elemental measures, namely $|B_k(\boldsymbol{e},\boldsymbol{\epsilon})|$ and $\|\boldsymbol{e}\|_k\ \|\boldsymbol{\epsilon}\|_k$, are distributed in similar fashions. Nevertheless, the latter choice gives a smoother distribution of error as clearly seen in the case of a linear mesh (i.e. Fig. 5). The error distributions agree well with the profile of the influence function shown in Fig. 4, suggesting that the residuals are distributed towards the end point of the plate where the boundary conditions change abruptly.

In this example, both h-factor and p-factor of the finite element discretization are investigated. We examine three meshes, each of which is combined with four orders of polynomial interpolation, ranging from linear interpolation ($p = 1$) to quartic interpolation ($p = 4$). The convergence trends of the norms of the displacement, the influence function and the quantity of interest are shown in Fig. 7. Apparently, all measures converge faster using the p-extension than the h-extension. Without surprise, the error estimates of the primal and the dual problem also follow the same trends, as shown in Fig. 8.

For goal-oriented convergence, four error measures, namely $|\mathscr{B}(e,\epsilon)|, \|e\|\|\epsilon\|, \sum_k|\mathscr{B}_k(e,\epsilon)|$ and $\sum_k(\|e\|_k\|\epsilon\|_k)$, are investigated. In Fig. 9, all error measures show the same trends of convergence. It is found that the sums of the elemental contributions (Subfigures (c) and (d)) are suitable representations of the global measures (Subfigures (a) and (b)). Providing straightforward contribution from the elemental error data, we trust that the newly proposed global quantities can result in an effective adaptive mesh discretization.

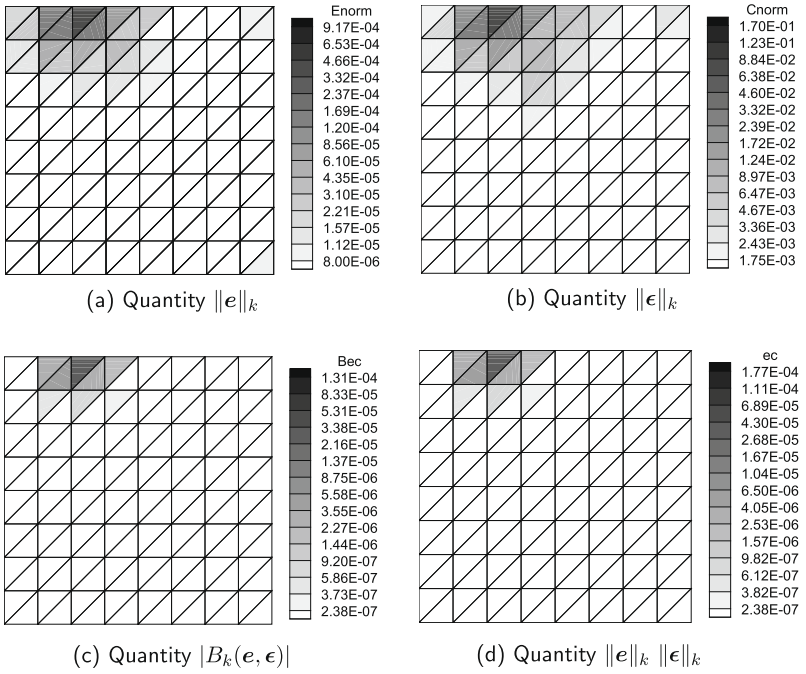

(a) Quantity $\|e\|_k$ (b) Quantity $\|\epsilon\|_k$

(c) Quantity $|B_k(e,\epsilon)|$ (d) Quantity $\|e\|_k\ \|\epsilon\|_k$

Fig. 6. Distribution of the elemental error measures in the framework of primal and dual problem, as well as the goal-oriented framework. The quadratic interpolation in Mesh 1 is employed. Exponential scaling is used.

5. Adaptive criteria

An objective of adaptive strategies is to provide a finite element solution with an acceptable level of discretization error. As such, criteria to judge whether or not the mesh is sufficiently discretized are needed. The criteria must be set such that the global error that is allowed to occur should be less than an acceptable value to guarantee an acceptable solution, and the local error should be well distributed throughout the problem domain. Furthermore, the mesh can be optimally designed, via an *h*-adaptive scheme, according to the mathematical derivation of the error in terms of its convergence with respect to the element sizes [13,21,20,24,42]. In this research, we choose to use the optimality criterion introduced in [21,20] as it can produce the cheapest mesh via the *a priori* local error estimate and the uniform error distribution. The criteria are also modified for use in goal-oriented framework.

5.1. Energy norm based adaptive criteria

By global consideration, the mesh needs an enhancement when

$$\|e\| > \zeta_{\text{prim}}\|u\|, \tag{44}$$

where ζ_{prim} is the amount of error allowed in comparison to the norm of the primary unknown u. If the global criterion is satisfied, the error in some regions of the problem domain may be higher than elsewhere. Basically, there are two principles to redistribute the error; based on *uniform error* distribution [42,21] or based on *uniform error density* distribution [17,24]. It has been found that using the uniform error density distribution leads to a much more expensive mesh than the uniform error distribution [13,24,5]. Since the uniform error distribution rule leads to acceptable results, in this study we will use this distribution principle.

By uniform error distribution, the elemental error reads

$$\|e\|_k^2 = \frac{\|e\|^2}{N} \forall\ k, \tag{45}$$

where N denotes the number of elements in the mesh. Combining this local criterion (cf. Eq. (45)) with the global criterion (cf. Eq. (44)), the mesh in the local region k must be enhanced when

$$\|e\|_k > \frac{\zeta_{\text{prim}}\|u\|}{\sqrt{N}}. \tag{46}$$

Following [21,20], the critical value of the error in energy norm reads

$$\|e\|_k = \mathscr{C}_{\text{prim}} h_k^{\frac{2p+d}{2}}, \tag{47}$$

which further leads to

$$\frac{\{h_k\}_{\text{des}}}{h_k} = \left(\frac{\{\|e\|_k\}_{\text{des}}}{\|e\|_k}\right)^{\frac{2}{2p+d}} = \left(\frac{\zeta_{\text{prim}}\|u\|}{\sqrt{N}\|e\|_k}\right)^{\frac{2}{2p+d}}, \tag{48}$$

where $\{h_k\}_{\text{des}}$ denotes the desired characteristic size of element k corresponding to the desired local error quantity $\{\|e\|_k\}_{\text{des}}$.

5.2. Goal-oriented adaptive criteria

In this research, to facilitate the combination of global and local refinement criteria, we have selected two global refinement criteria.

5.2.1. Adaptive criterion 1

Whenever

$$\sum_{k=1}^{N} |B_k(e,\epsilon)| > \zeta_{\text{goal}} \sum_{k=1}^{N} |B_k(u,w)|, \tag{49}$$

the mesh needs to be improved. It is noted that the measure $|B_k(u,w)|$ is not equal to zero as in the global measure $|B(u,w)|$ in the displacement control algorithm. Similar to the distribution of error in the energy norm, the error measure can be distributed uniformly as

$$|B_k(e,\epsilon)| = \frac{\sum_{j=1}^{N} |B_j(e,\epsilon)|}{N} \forall\ k. \tag{50}$$

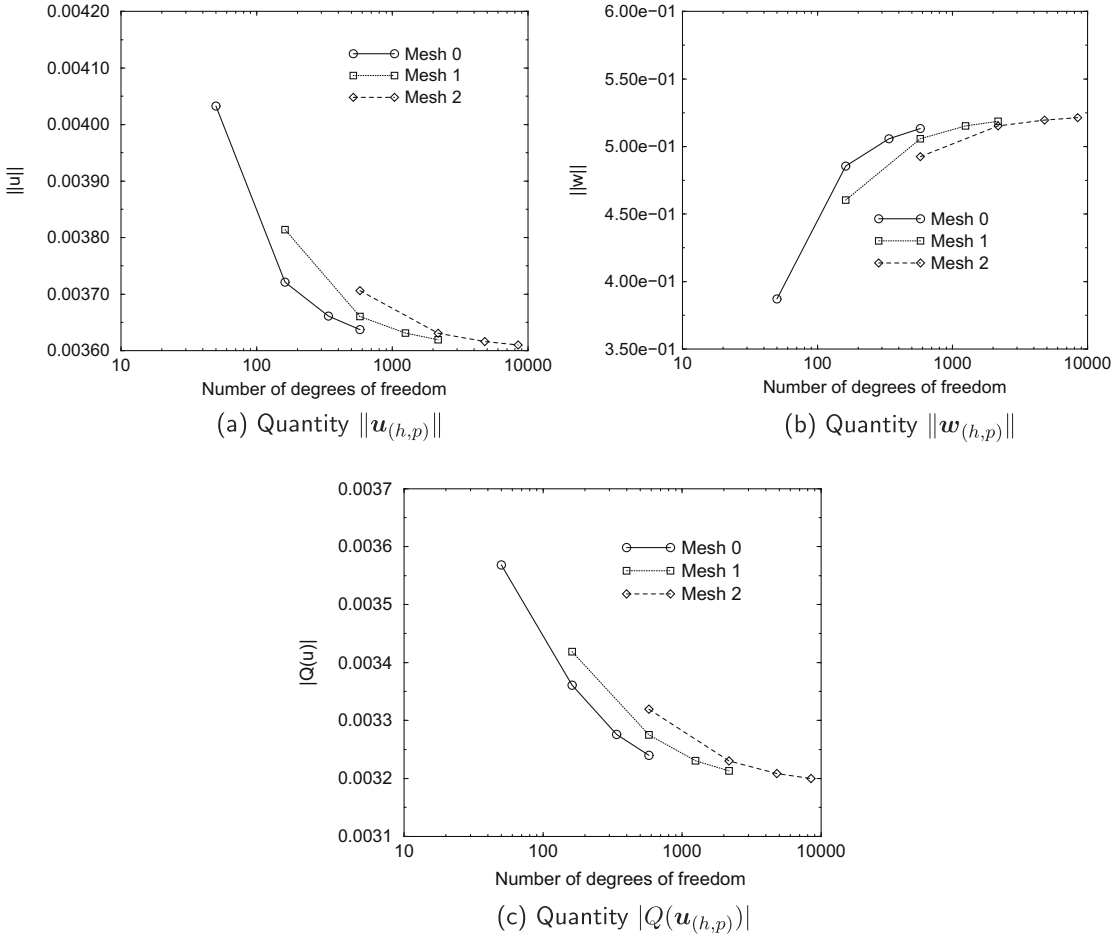

Fig. 7. Global convergence of the solutions in the primal problem, the solutions in the dual problem and the goal quantity.

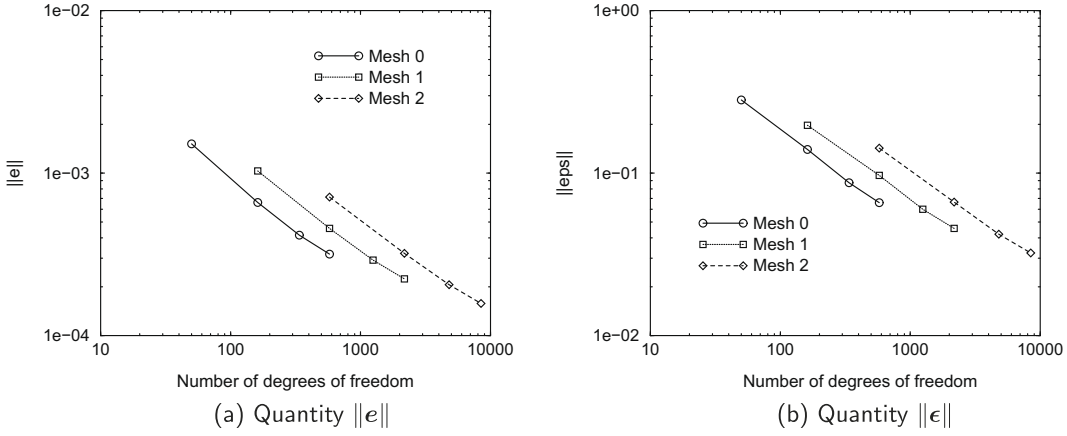

Fig. 8. Energy norm of error in primal and dual problem.

And by combining this local criterion with the global criterion, the mesh in the local region k must be enhanced when

$$|B_k(e,\epsilon)| > \frac{\zeta_{\text{goal}}\sum_{j=1}^{N}|B_j(u,w)|}{N}. \tag{51}$$

The relative element size can be optimally set as

$$\frac{\{h_k\}_{\text{des}}}{h_k} = \left(\frac{\{|B_k(e,\epsilon)|\}_{\text{des}}}{|B_k(e,\epsilon)|}\right)^{\frac{1}{2p+d}} = \left(\frac{\zeta_{\text{goal}}\sum_{k=1}^{N}|B_k(u,w)|}{N_{\text{new}}|B_k(e,\epsilon)|}\right)^{\frac{1}{2p+d}}. \tag{52}$$

5.2.2. Adaptive criterion 2

The mesh needs to be improved whenever

$$\sum_{k=1}^{N}(\|e\|_k\|\epsilon\|_k) > \zeta_{\text{goal}}\sum_{k=1}^{N}(\|u\|_k\|w\|_k). \tag{53}$$

Again, the error measure can be distributed by uniform error distribution

$$\|e\|_k\|\epsilon\|_k = \frac{\sum_{j=1}^{N}(\|e\|_j\|\epsilon\|_j)}{N}\forall\ k. \tag{54}$$

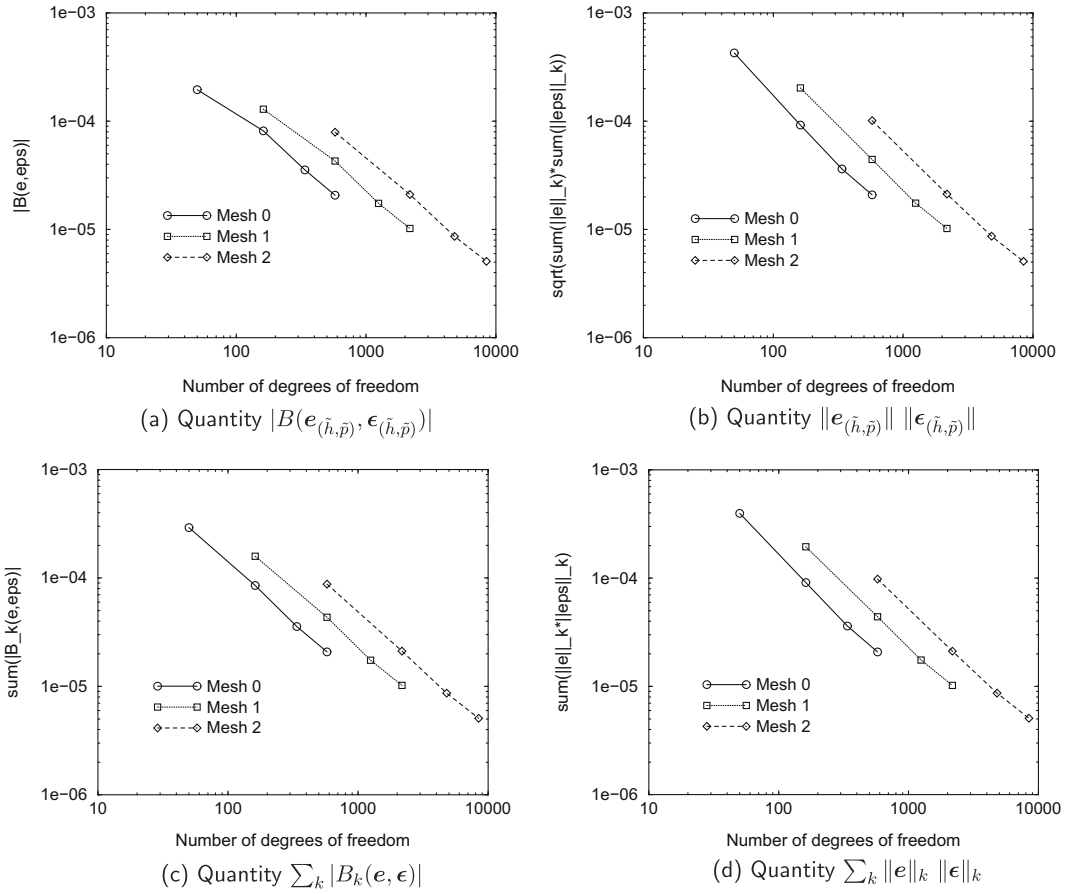

Fig. 9. Comparison of various goal-oriented measures.

Combining this local criterion with the global criterion, the mesh in the local region k must be enhanced when

$$\|e\|_k\|\epsilon\|_k > \frac{\zeta_{\text{goal}}\sum_{j=1}^{N}(\|u\|_j\|w\|_j)}{N}. \tag{55}$$

The relative element size is optimally cast as

$$\frac{\{h_k\}_{\text{des}}}{h_k} = \left(\frac{\{\|e\|_k\|\epsilon\|_k\}_{\text{des}}}{\|e\|_k\|\epsilon\|_k}\right)^{\frac{1}{2p+d}} = \left(\frac{\zeta_{\text{goal}}\sum_{k=1}^{N}(\|u\|_k\|w\|_k)}{N_{\text{new}}\|e\|_k\|\epsilon\|_k}\right)^{\frac{1}{2p+d}}. \tag{56}$$

Apparently, the global allowance in the framework of goal-oriented error estimation ζ_{goal} can be set as

$$\zeta_{\text{goal}} \approx \zeta_{\text{prim}}\zeta_{\text{dual}}, \tag{57}$$

where ζ_{prim} and ζ_{dual} are global allowances for the error in the primal problem and for the error in the dual problem, respectively.

6. Numerical examples

The theoretical settings of the previous sections are now applied to two numerical examples. As our main objective, we would like to measure the discretization error in the modelling of continuous failure (using the gradient-enhanced damage model) and use this study as preliminary information for formulating adaptive strategies.

Note that, in both examples, we consider a loading with incremental displacement, since the problems show a softening behavior which cannot be captured when using a force-driven algorithm.

6.1. Central transverse crack test

The first numerical example is the central transverse crack test, described in Fig. 10. Due to symmetry, only the upper right quarter is modelled under a plane stress condition. We apply the displacement control algorithm with a proportionally prescribed displacement of $\overline{u} = 0.00001$ mm for each incremental step in the Newton–Raphson iterative scheme. To investigate the h-factor of the finite element discretization, we select three uniform triangular meshes, namely Mesh 0, Mesh 1 and Mesh 2 as given in Fig. 11. For investigation of the p-factor, four orders of interpolation, ranging from linear order ($p = 1$) to quartic order ($p = 4$), are applied in a hierarchical manner. Details of these reference meshes are given in Table 1.

6.1.1. Effects of mesh discretization on FE solutions

To examine the effects of mesh discretization on the finite element results, preliminary tests are carried out based on uniform meshes with uniform orders of interpolation. It is shown in Fig. 12(left) that the load–displacement relation for the coarsest mesh (Mesh 0) with linear interpolation ($p = 1$) is significantly different from the rest of the results. We observe that the finite element computation is likely to overestimate the reaction forces corresponding to the prescribed displacements. Both h-factor and p-factor can, indeed, improve the accuracy of the solution in this global sense. As an additional observation in Fig. 12(right), the response obtained by p-extension is observed to improve the finite element solution faster than the h-extension.

We select Mesh 2 with quartic interpolation to describe evolution of the damage parameter and the equivalent strain during the

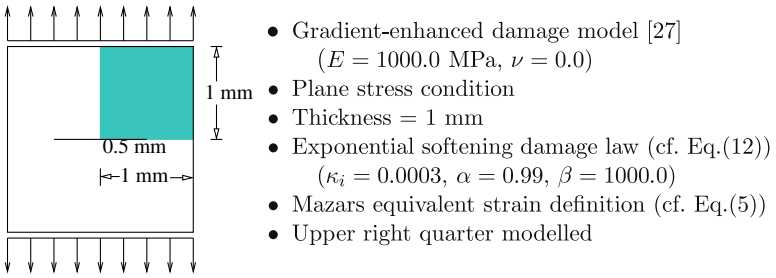

Fig. 10. The central transverse crack test.

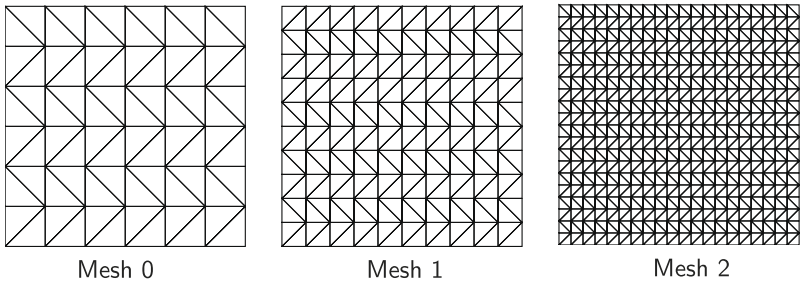

Fig. 11. Meshes used in the finite element analysis of the central transverse crack test.

Table 1
Information of fixed meshes used in the central transverse crack test.

Mesh	No. of nodes	No. of elements	p-order	NDOFs
0	49	72	1	147
			2	507
			3	1083
			4	1875
1	121	200	1	363
			2	1323
			3	2883
			4	5043
2	441	800	1	1323
			2	5043
			3	11163
			4	19683

softening process. It is evident that damage appears initially before the peak load is reached (precisely, Step 26 or $\overline{u} = 0.00026$ mm). The material is still able to carry more load up to Step 30 ($\overline{u} = 0.00030$ mm), followed by global softening. In Fig. 13, it can be seen that, in the post-peak regime, the strain localizes where the damage grows.

Profiles of the damage and the equivalent strain at a cut section $x = 1.0$ mm, shown in Fig. 14, reveal the influence of mesh discretization in the damage analysis. The meshes under investigation are Mesh 1 and Mesh 2 with linear and quadratic interpolations. We compare two mesh improvement approaches by upgrading Mesh 1 with linear interpolation using similar additional numbers of degrees of freedom (i.e. Mesh 1 with quadratic interpolation and Mesh 2 with linear interpolation). As can be seen in Fig. 12(left), both the h-factor and the p-factor can improve the damage and equivalent strain profiles at the selected cut section. Nevertheless,

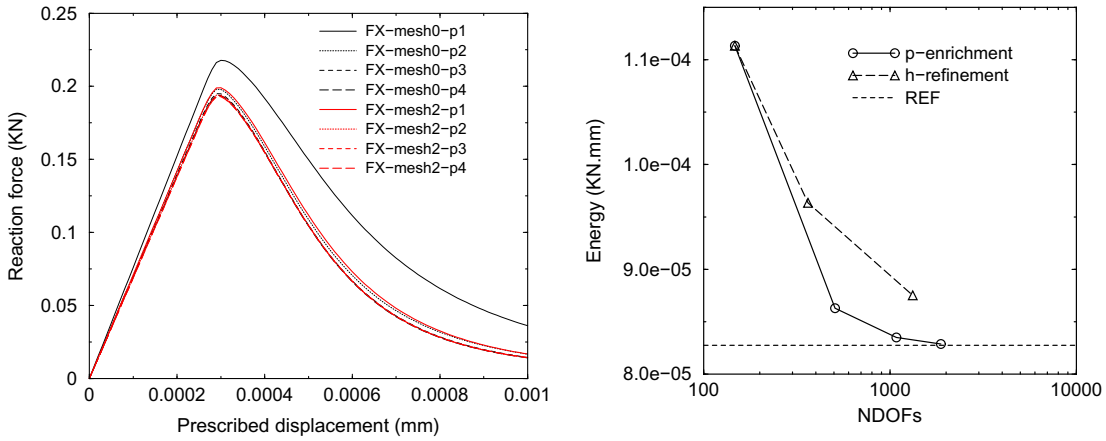

Fig. 12. Load–displacement relations (left) and corresponding dissipated energy (right) for the central transverse crack test. The abbreviation FX refers to the fixed computational mesh, i.e. no mesh adaptivity is activated. The abbreviation REF denotes the result obtained from the reference mesh, i.e. Mesh 2 with quartic interpolation.

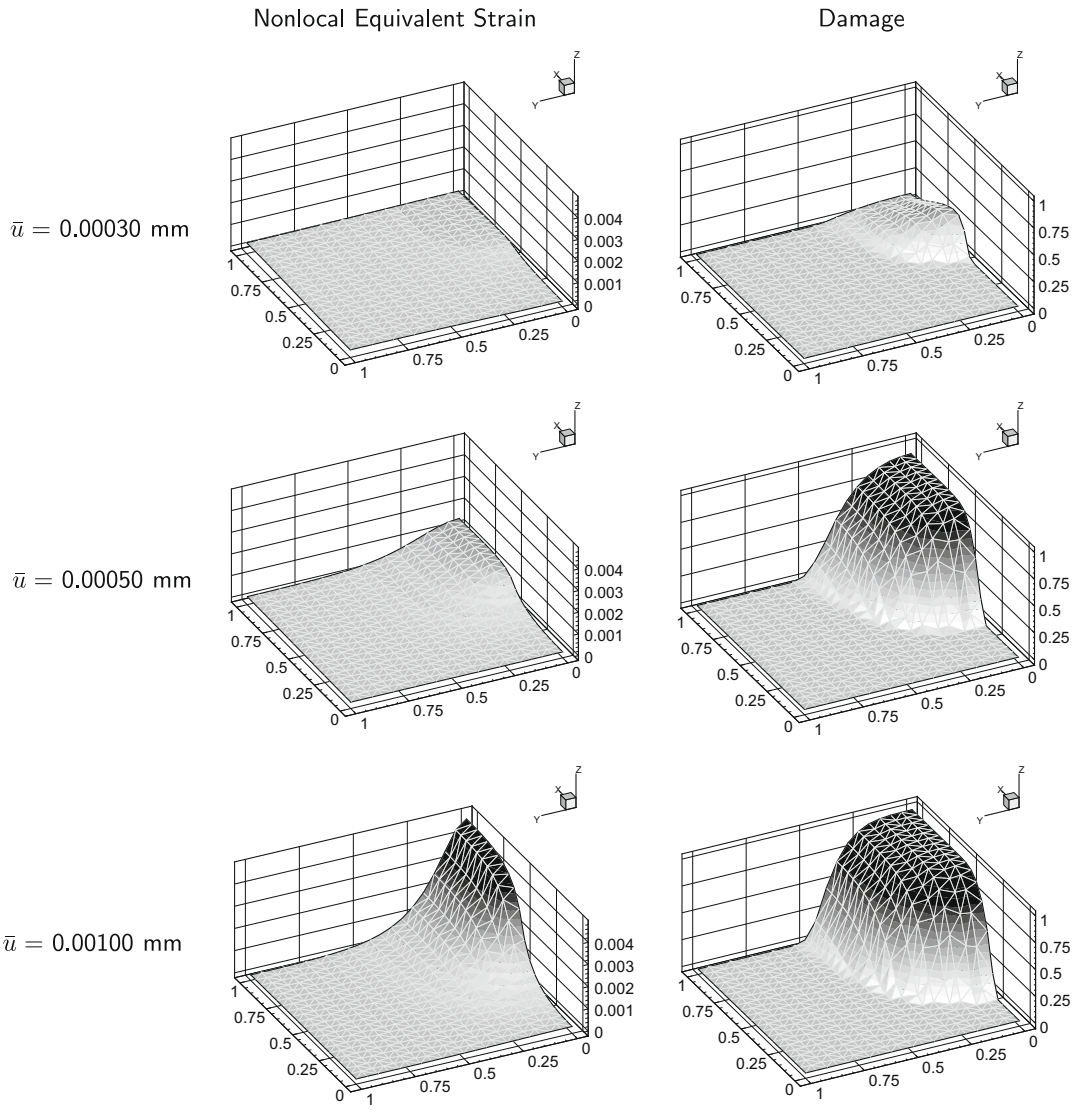

Fig. 13. Evolution of nonlocal equivalent strain and damage obtained from Mesh 2 with quartic interpolation.

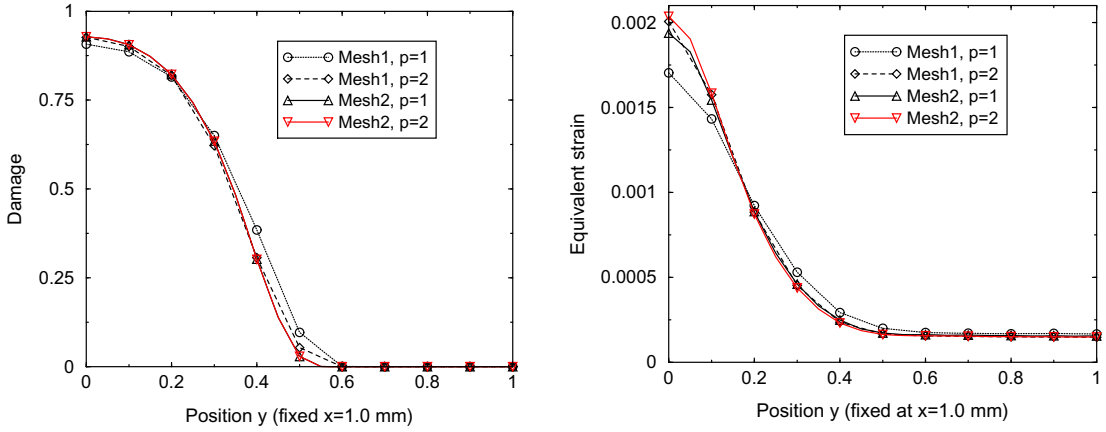

Fig. 14. Profiles of damage parameter and equivalent strain measured along the $x = 1.0$ mm when $\bar{u} = 0.00050$ mm.

improving the mesh by applying higher-order interpolation depends largely on the topology of the mesh. If the mesh possesses an insufficient resolution at the region of high-gradient solutions, using higher-order interpolation (p-factor) can only improve the local solution up to a limited extent.

6.1.2. Analysis of error information

As mentioned in the previous sections, we estimate the errors of all primary unknowns in the discretized equations. Recalling Eq. (29), the total error estimate $\|e\|^+$ consists of two independent contributions, namely the error in the displacement field $\|e_u\|^+$ and the

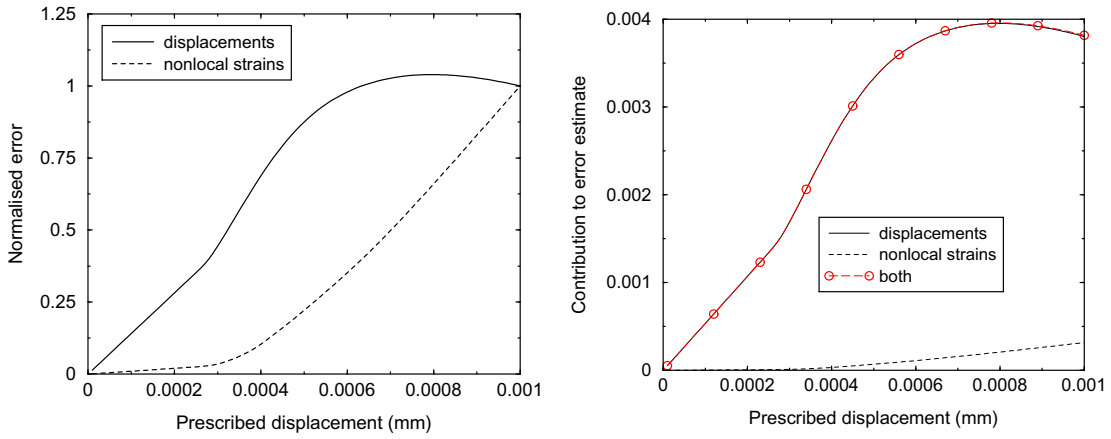

Fig. 15. Contribution of all degrees of freedom to norm measure, using Mesh 1 with linear interpolation.

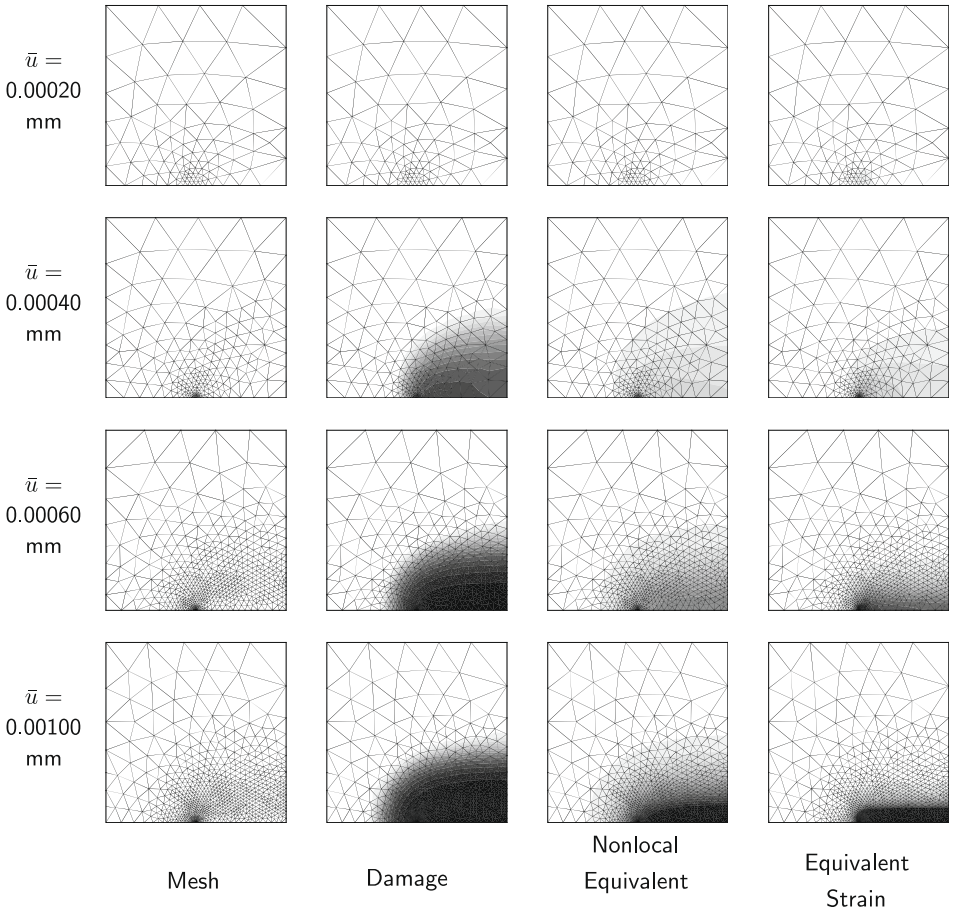

Fig. 16. Meshes used during the *h*-adaptivity Scheme 1 and the corresponding state variables during computation. The computation is continued after variable transfer by the closest point approach [26].

error in the nonlocal equivalent strain field $\|e_{\bar{\varepsilon}}\|^+$. These two contributions to the error estimate do not have the same dimension, thus the computed error norm is no longer an energy measure. However, by the fact that both unknown fields are discretized and solved via finite element analysis, both contributions should be taken into account in the error analysis.

Fig. 15 shows individual contributions of the error estimates obtained at the end of each loading step in the finite element computation. To observe the trend of both error contributions, in Fig. 15(left), we present each contribution by normalising it with respect to the value at the end of the loading process ($\bar{u} = 0.001$ mm). It appears that both contributions increase at higher rates after the peak in the load–displacement response is reached. This does not hold anymore towards the end for the displacements, where the estimated error is decreasing.

It is, however, observed in Fig. 15(right) that the error in the nonlocal equivalent strain field provides a much smaller contribution to the total error measure than the one in the displacement

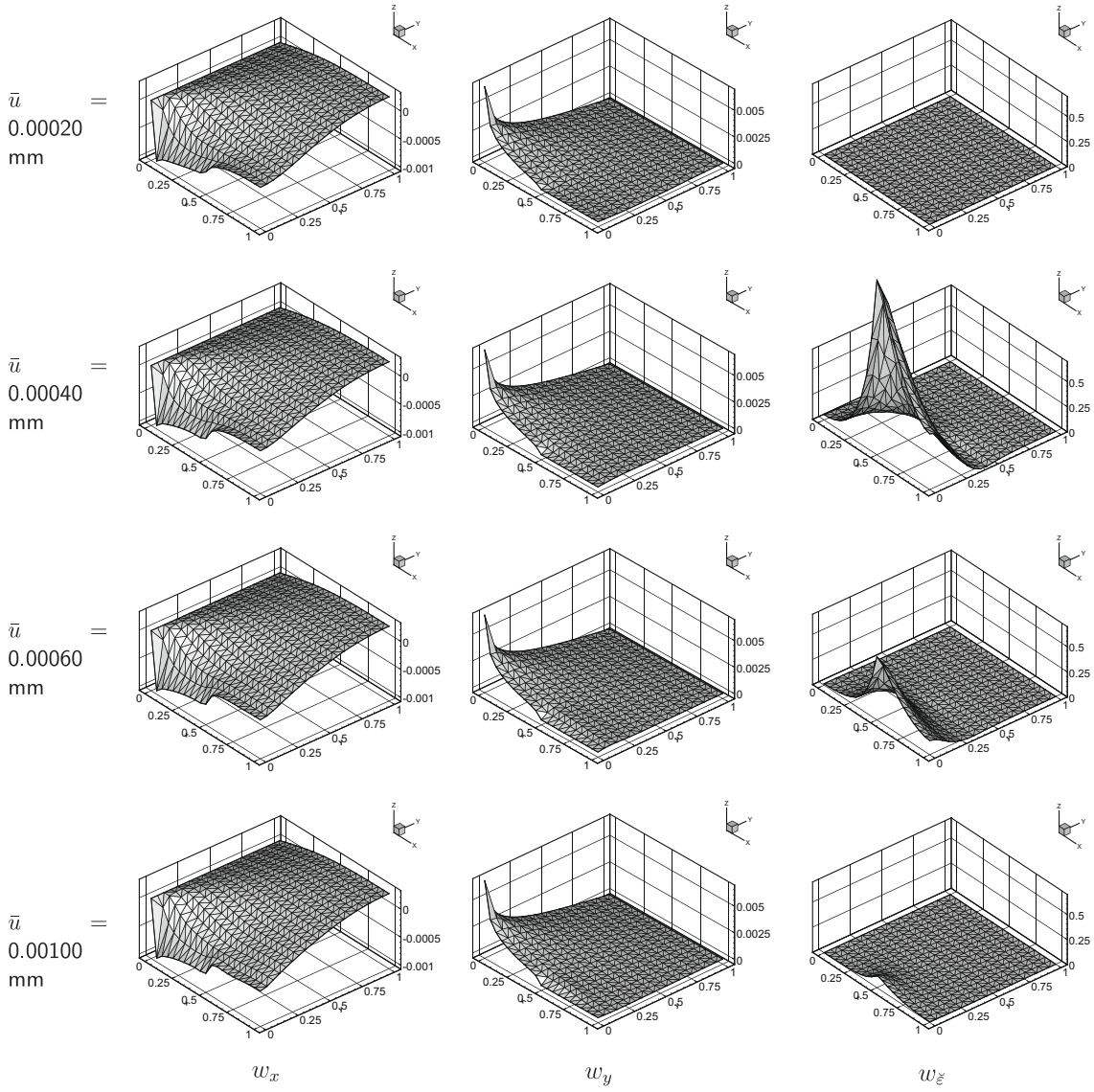

Fig. 17. Influence functions corresponding to the crack opening displacement, obtained from Mesh 2 with quadratic interpolation.

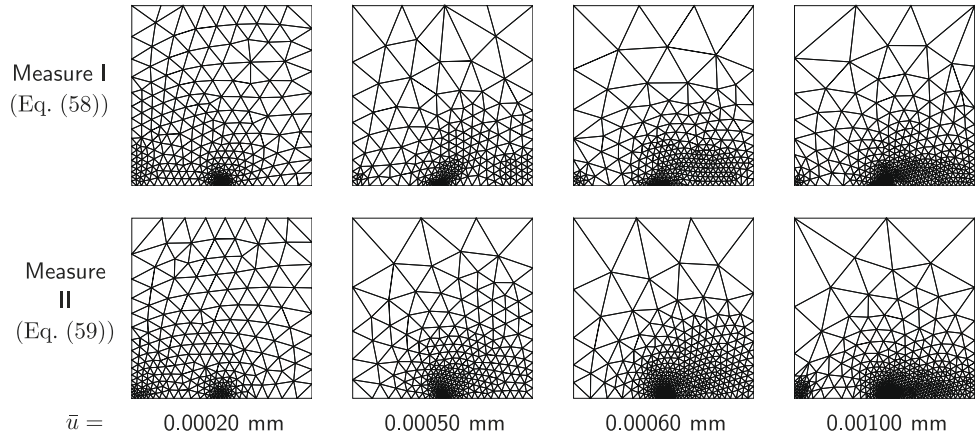

Fig. 18. Meshes obtained during the goal-oriented *h*-adaptivity.

field. Note that this is not caused by the different dimensions of the two solutions since each is normalized separately prior to this summation. Thus, an economical alternative of this error estimation would be to assess the error in the displacement field only, disregarding the error in the nonlocal equivalent strain field. Despite this observation, we employ in this study the contributions

of both fields in estimating the error of the finite element computation.

6.1.3. Automated mesh adaptivity

In this test, the discretization error is approximated at the end of each numerical step. Filtered by the adaptive criteria (cf. Section 5), some regions in the finite element mesh may be improved via mesh adaptivity. We control the error not to be beyond 15% of the solution norm.

In this study, *h*-adaptivity is chosen. The element sizes can be designed via the optimality criterion relying on the *a priori* convergence assumption (cf. Section 5). The discretization error is measured at the end of each computational step to make sure that the error information is more relevant to where the discretization is particularly needed at that stage of the computation. Filtered by the adaptive criteria, the mesh may be totally adapted and the history variables are transferred using the closest point technique [26]. The evoluting meshes and the corresponding state variables are shown in Fig. 16.

In this study, the performance of the goal-oriented adaptive computation is also investigated. We choose here the crack mouth opening displacement (CMOD) as our quantity of interest. A half of this quantity can be measured as the displacement in the *y*-direction at the lower left corner of the problem domain. As a reasonable assumption, the dual problem is set as a stationary linear problem at any computational step. At some selected computational steps, three sets of influence functions (corresponding to 3 degrees of freedom used in the implicit gradient-enhanced damage formulation) of the crack mouth opening displacement are shown in Fig. 17.

We separate the discretization residual into three parts, corresponding to each degree of freedom, i.e. r_x, r_y and $r_{\breve{\varepsilon}}$ correspond to u_x, u_y and $\breve{\varepsilon}_{\text{eq}}$, respectively. It is found that a unit change of r_x and r_y consistently affects the CMOD, while a unit change of $r_{\breve{\varepsilon}}$ varies its influence on the CMOD during the loading process. A unit change in $r_{\breve{\varepsilon}}$ before the peak (i.e. at $\bar{u} = 0.00020$ mm) does not have any influence on the CMOD. However, once the strain starts to localize, the influence of $r_{\breve{\varepsilon}}$ concentrates at the crack tip (i.e. at $\bar{u} = 0.00040$ mm) and distributes in a more uniform fashion in the damaged region in the later stage (i.e. at $\bar{u} = 0.00060$ mm and $\bar{u} = 0.00100$ mm).

After the influence functions are obtained, the error in the specific quantity (i.e. CMOD) is measured. Fig. 18 shows the meshes used during goal-oriented *h*-adaptivity, where two error measures

$$\text{Measure I } \mathscr{E}_k^I := |\mathscr{B}_k^{\text{tang}+}(\breve{\boldsymbol{e}}, \breve{\epsilon})|, \tag{58}$$

$$\text{Measure II } \mathscr{E}_k^{II} := \|\breve{\boldsymbol{e}}\|_k^{\text{tang}+} \|\breve{\boldsymbol{\epsilon}}\|_k^{\text{tang}+}, \tag{59}$$

are compared. Though different, the mesh designs based on both measures also show some similarities. It is evident that, in the linear-elastic regime, accuracy of the crack mouth opening displacement (as our goal quantity) depends greatly on the discretization at the point of interest and at the crack tip where there exists a stress singularity. On the other hand, the discretization in the process zone (damage zone) becomes more demanding in the later stage when damage emerges.

The only difference clearly seen between the two measures is that, in the softening regime, Measure I detects an outstanding amount of error at the crack mouth while the error in that region does not appear significant with Measure II. This may be explained by the mathematical definitions of the two measures: there is a multiplicative contribution of the error of both problems in Measure I, while Measure II separates the error of the primal problem and the error of the dual problem.

Note that goal-oriented adaptivity is controlled by threshold value ζ_{goal} (cf. Section 5.2) for both measures, which is taken not to be more than 2.25%.

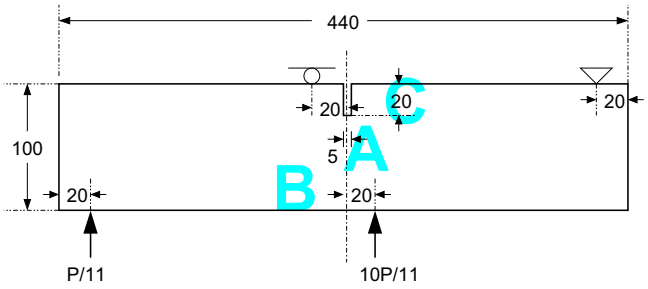

Fig. 19. The single-edge-notched (SEN) beam, with dimension in millimeters.

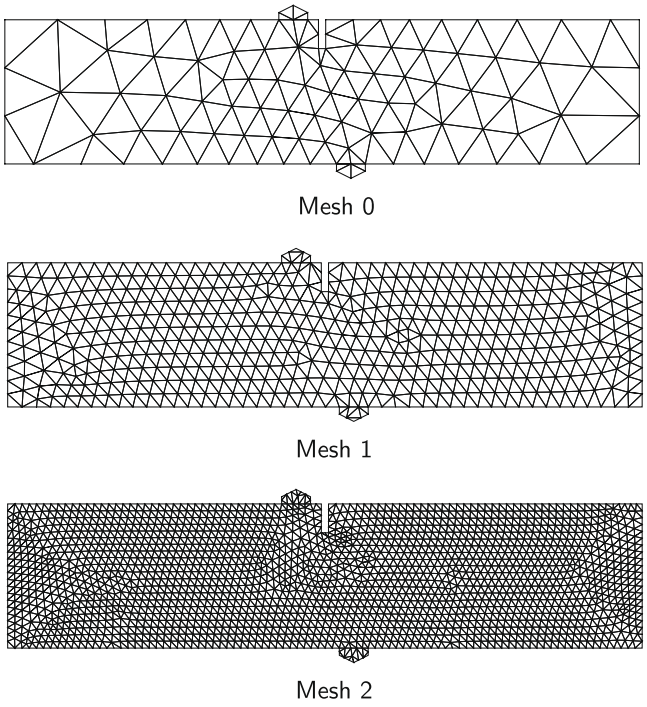

Fig. 20. Meshes used in the finite element analysis of the SEN beam.

Table 2
Information of fixed meshes used in the SEN beam computation.

Mesh	No. of nodes	No. of elements	*p*-order	NDOFs
0	107	159	1	321
			2	1116
			3	2388
			4	4137
1	534	938	1	1602
			2	6015
			3	13242
			4	23283
2	1978	3709	1	5934
			2	22992
			3	51177
			4	90489

6.2. Single-edge-notched (SEN) beam test

Our second test is the single-edge-notched beam [38] whose geometrical details are given in Fig. 19. The material parameters used in this analysis are: Young's modulus $E = 30{,}000$ MPa, Poisson's ratio $\nu = 0.2$, gradient parameter $c = 0.3$ mm^2, modified von Mises equivalent strain definition (cf. Eq. (7)) with $k = 13.55$

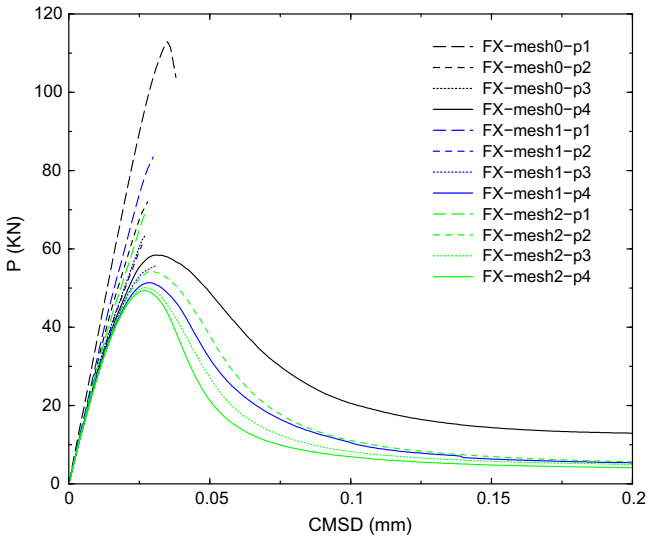

Fig. 21. Load–displacement relations for the SEN beam.

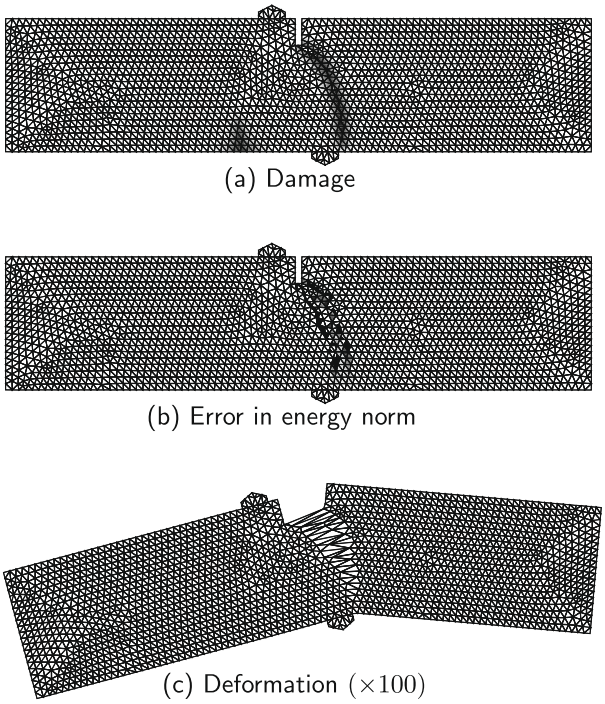

Fig. 22. The damage profile, the error distribution and the deformation obtained by using Mesh 2 with quartic interpolation in Step 125 (CMSD = 0.125 mm).

and exponential softening law (cf. Eq. (12)) with $\kappa_0 = 0.000115, \alpha = 0.96$ and $\beta = 100$. The beam, with a specified thickness of 100 mm, is analysed under a plane stress condition.

The beam is subjected to a skew-symmetric four-point shear loading, which is applied by means of an indirect displacement control. As the control parameter, an incremental crack mouth sliding displacement of 0.001 mm is applied per computational step in the full Newton–Raphson iterative scheme.

6.2.1. Analysis of error information

To investigate the *h*-factor and the *p*-factor of the finite element discretization, we select three uniform triangular meshes, namely

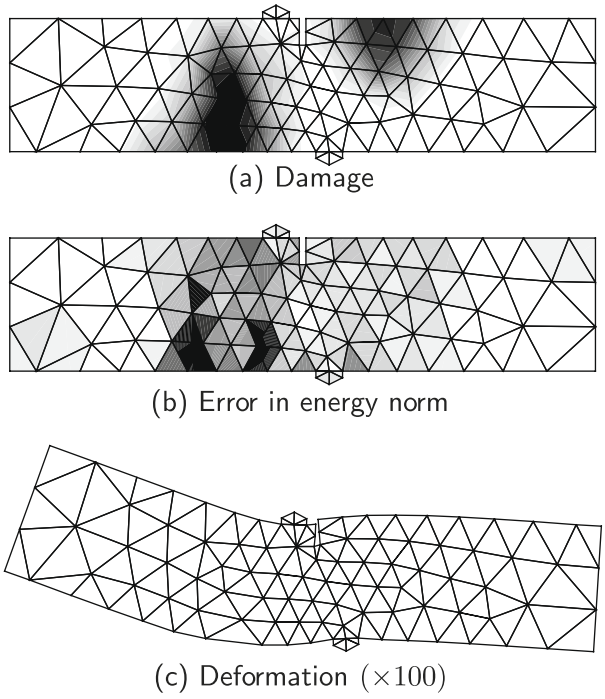

Fig. 23. The damage profile, the error distribution and the deformation obtained by using Mesh 0 with linear interpolation in Step 38 (CMSD = 0.038 mm).

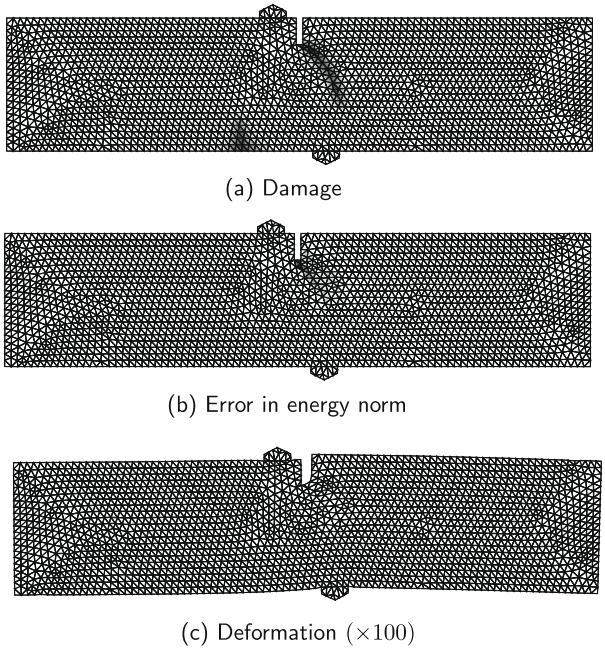

Fig. 24. The damage profile, the error distribution and the deformation obtained by using Mesh 2 with quartic interpolation in Step 38 (CMSD = 0.038 mm).

Mesh 0, Mesh 1 and Mesh 2 (cf. Fig. 20). Again, four orders of interpolation ($p = 1$ to $p = 4$) are applied. Table 2 presents some details of these reference meshes. The reference meshes are investigated first. The tests are carried out to examine the influence of the mesh resolution (*h*-factor) and the interpolation degree (*p*-factor) on the finite element solutions of the SEN beam modelling.

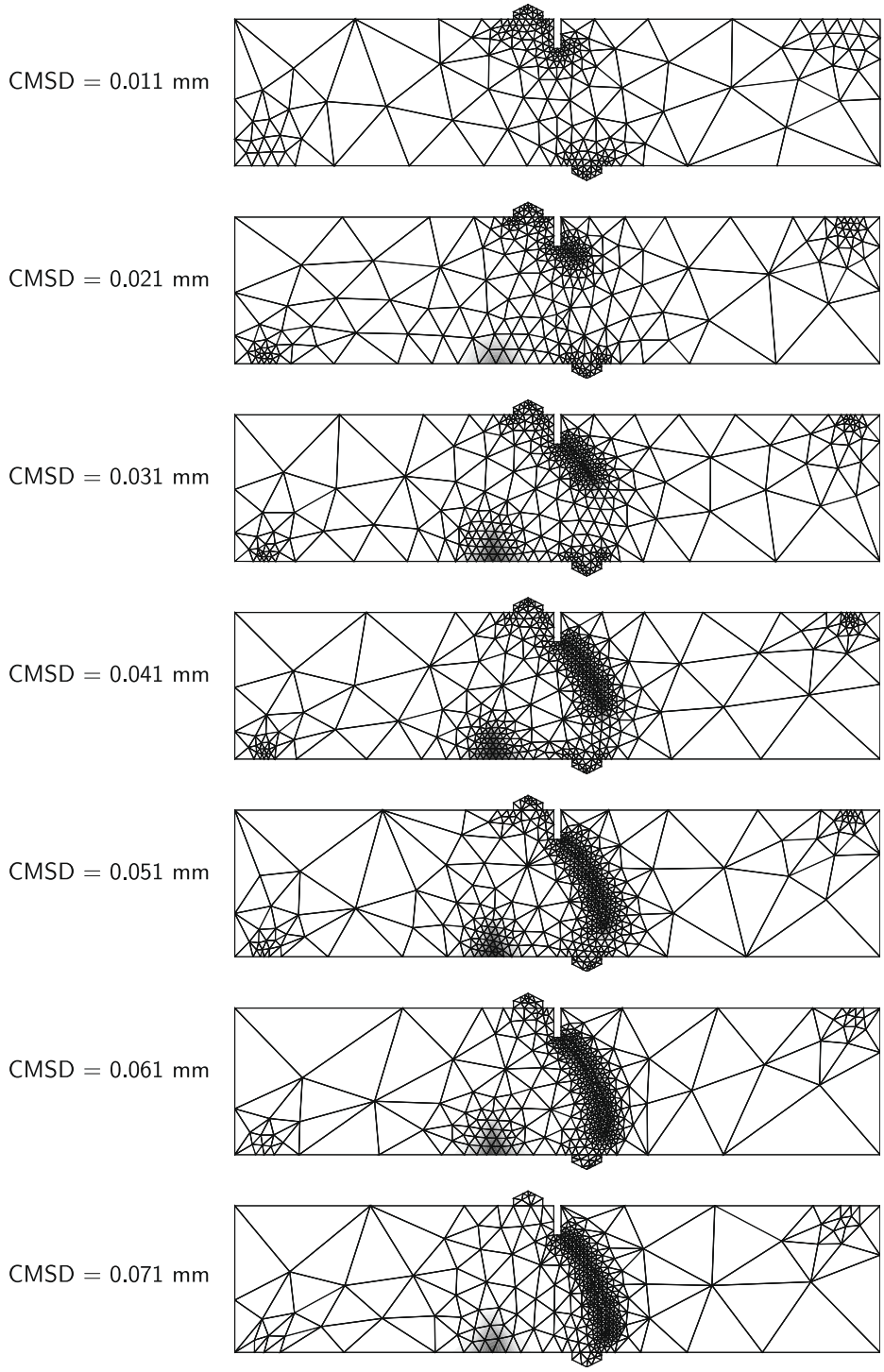

Fig. 25. Damage evolution and corresponding *h*-adaptivity in the SEN beam.

The load–displacement responses obtained from those reference meshes are plotted in Fig. 21. The finite element computations obviously fail when applying Mesh 0 and Mesh 1 with an interpolation order of less than four (quartic interpolation). It is also found that, with linear interpolation, even the finest mesh in the test (Mesh 2) leads to failure of the computation. The computational failure occurs, apparently, before the softening process starts and cannot be avoided by reducing size of the incremental load. These inadequate discretizations trigger incorrect failure mechanisms.

From Fig. 21, some further remarks are observed at two different stages.

- In the pre-peak stage, a less stiff response and subsequently a smaller load-carrying capacity (ultimate load) are noticed, upon mesh refinement and mesh enrichment. Considering the same number of degrees of freedom, increasing the interpolation order (mesh enrichment) provides faster convergence than refining the mesh.
- In the post-peak stage, a more brittle softening response is obtained upon mesh refinement and mesh enrichment. In contrast to the early stage, however, reducing element sizes results in a better performance than enriching the interpolation. The result is not surprising since it agrees with what we have found

in the previous example and also in literature [26,2]. A sufficient mesh resolution is clearly needed when the strain is more localized.

It is expected that damage may appear at three possible zones, namely

- Zone A, where the stress singularity is expected at the notch
- Zone B, where the maximum bending stress is expected
- Zone C, where a high bending stress is expected

as marked in Fig. 19. With the material parameters set in this test, we find that damage at the central zone (Zone A) is dominant and leads to failure of the beam, whereas damage at Zone B only grows to a limited extent. We do not find any damage in Zone C in our reference Mesh 2 with quartic interpolation. Plotted at Step 125 (CMSD = 0.125 mm), Fig. 22 shows the damage profile, the deformation and the error that seems to concentrate on the boundary of the primary damaged zone where the high strain gradients exist.

The situation is different when the discretization is not sufficient. Using Mesh 0 with linear interpolation, cracks at Zone B and Zone C appear to be dominant, whereas no damage is detected at Zone A. This wrong result subsequently leads to the appearance of the discretization error at Zone B where there exist high strain gradients, as shown Fig. 23 for Step 38 (CMSD = 0.038 mm). Now, imagine if we use the results obtained from Mesh 0 at this final step to consider where adaptivity should take place. Obviously, the error leads to wrong information (see Fig. 23(b)) and the adapted mesh will be completely inadequate. To obtain the correct information about adaptivity, it is clear that the mesh should be updated during the loading process. See Fig. 24 for a comparison with the reference discretization (Mesh 2 with quadratic interpolation) at the same step.

6.2.2. Automated mesh adaptivity

Similar to the central transverse crack test, we allow 15% of the error measure to be present in the analysis. Due to the complexity of the SEN beam problem, the FE analysis requires more computational cost than it does in the previous example. Instead of computing error and activating adaptivity at every step of computation, we activate the processes every 10 steps, in order to get reasonable updates of the mesh balanced with the demands on computational efforts. With the total CMSD subdivided in 200 increments, this implies 20 possible adaptive processes during the entire analysis. In Fig. 25, the evolution of the mesh is shown.

We start the use of *h*-adaptivity with Mesh 0 with quartic interpolation. We prevent excessive refinement by specifying the possible element size not to be smaller than the minimum value, which in this test is half of the element size of Mesh 2.

Compared with the results from the reference meshes, it is shown in Fig. 26 that the result from the *h*-adapted mesh almost duplicates the result of Mesh 2. Actually, when smaller element sizes than those in Mesh 2 are applied at the critical zones, a softer behavior is obtained in the adapted mesh. Considering the computational cost, the number of degrees of freedom used in the adapted case varies during the loading process. The result also reveals that the maximum number of degrees of freedom used in the computation is 21,099, while in Mesh 2 without any adaptivity, this number is more than four times as much.

7. Concluding remarks

The error estimator presented in [25] has been applied to a gradient-enhanced damage model. The error measures, which are based on the positive-definite part of the stiffness matrix, include those in a solution norm and in a specific quantity, i.e. the crack mouth opening displacement. To seek the most suitable mesh discretization for the model, the *h*-factor and the *p*-factor have been studied.

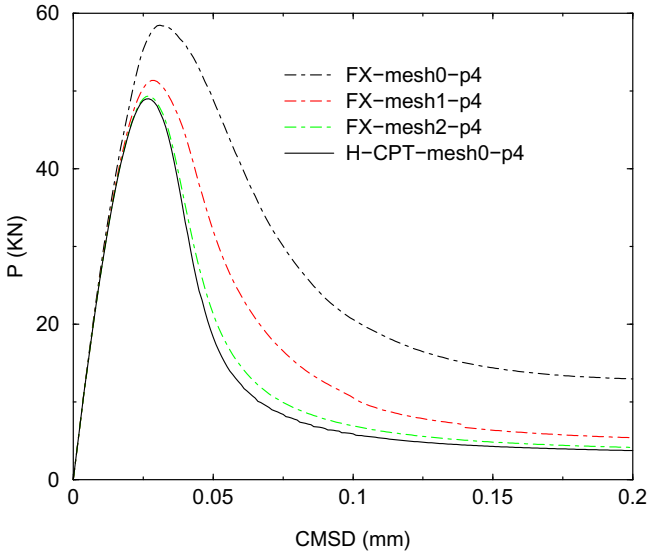

Fig. 26. Load–CMSD relations for the SEN test with *h*-adaptivity.

In the study, we have found that the discretization error in the linear-elastic regime appears to concentrate at the supports and the notches (where there exists stress singularities). Once damage is initiated, the error in the damage zone appears to take more control. During the loading process, a sufficiently refined or enriched discretization is obviously needed in the zone of high strain gradient, which is usually the zone where damage appears. However, containing the highest damage level does not mean that the zone needs the most refined/enriched discretization. As a good alternative to the error estimation, an error indication, after the damage is initiated, could be the gradient of the equivalent strain or of its nonlocal counterpart, rather than the damage level. We have also found that the error in the nonlocal equivalent strain field provides a much smaller contribution to the total error measure than the one in the displacement field. Thus, an economical alternative of this error estimation would be to assess the error in the displacement field only. Furthermore, via goal-oriented adaptivity based on crack mouth opening displacement, we have also observed in the punch test that, once the damage appears, correct modelling of the damage and the strain profiles also guarantees accuracy of the specific quantity.

Once the error information is at hand, the adaptive process is activated when the global error exceeds a user-specified global error allowance. Based on uniform error distribution, the process takes place in the regions of large elemental errors. With the adaptive process activated during the computation, the cracking process is ensured to follow a correct path with a realistic width of the process zone.

References

[1] M. Ainsworth, J.T. Oden, A Posteriori Error Estimation in Finite Element Analysis, John Wiley and Sons, 2000.
[2] H, Askes, Advanced Spatial Discretisation Strategies for Localised Failure: Mesh Adapivity and Meshless Methods, Ph.D. Thesis, Delft University of Technology, The Netherlands, 2000. <http://www.library.tudelft.nl/dissertations>.
[3] H. Askes, L.J. Sluys, Remeshing strategies for adaptive ALE analysis of strain localisation, Eur. J. Mech. A: Solids 19 (2000) 447–467.
[4] R. Becker, R. Rannacher, Feed-back approach to error control in finite element methods: basic analysis and examples, East-West J. Numer. Math. 4 (1996) 237–264.

[5] G. Bugeda, A comparison between new adaptive remeshing strategies based on point wise stress error estimation and energy norm error estimation, Commun. Numer. Methods Engrg. 18 (2002) 469–482.
[6] L. Chamoin, P. Ladevèze, Goal-oriented error estimation and adaptivity for the finite element method, Comput. Math. Appl. 41 (2001) 735–756.
[7] F. Cirak, E. Ramm, A posteriori error estimation and adaptivity for linear elasticity using the reciprocal theorem, Comput. Methods Appl. Mech. Engrg. 156 (1998) 351–362.
[8] F. Cirak, E. Ramm, A posteriori error estimation and adaptivity for elastoplasticity using the reciprocal theorem, Int. J. Numer. Methods Engrg. 47 (2000) 379–393.
[9] C. Comi, U. Perego, Criteria for mesh refinement in nonlocal damage finite element analyses, Eur. J. Mech. A: Solids 23 (2004) 615–632.
[10] J.H.P. deVree, W.A.M. Brekelmans, M.A.J. van Gils, Comparison of nonlocal approaches in continuum damage mechanics, Comput. Struct. 55 (1995) 581–588.
[11] P. Díez, M. Arroyo, A. Huerta, Adaptivity based on error estimation for viscoplastic softening materials, Mech. Cohes. Frict. Mater. 5 (2000) 87–112.
[12] P. Díez, J.J. Egozcue, A. Huerta, A posteriori error estimation for standard finite element analysis, Comput. Methods Appl. Mech. Engrg. 163 (1998) 141–157.
[13] P. Díez, A. Huerta, A unified approach to remeshing strategies for finite element *h*-adaptivity, Comput. Methods Appl. Mech. Engrg. 176 (1999) 215–229.
[14] P. Díez, I. Morata, A. Huerta, Goal-oriented adaptivity for shell structures: error estimation and remeshing criteria, Revue Européenne des Éléments Finis 12 (2003) 691–715.
[15] P. Heintz, F. Larsson, P. Hansbo, K. Runesson, On error control and adaptivity for computing material forces in fracture mechanics, in: WCCM V – Fifth World Congress on Computational Mechanics, Vienna, Australia, 2002. <http://wccm.tuwien.ac.at>.
[16] P. Heintz, K. Samuelsson, On adaptive strategies and error control in fracture mechanics, Comput. Struct. 82 (2004) 485–497.
[17] A. Hernández, J. Albizuri, M.B.G. Ajuria, M.V. Hormaza, An adaptive meshing automatic scheme based on the strain energy density function, Engrg. Comput. 14 (1997) 604–629.
[18] P. Ladevèze, N. Moës, B. Douchin, Constitutive relation error estimator for (visco)plastic finite element analysis with softening, Comput. Methods Appl. Mech. Engrg. 176 (1999) 247–264.
[19] F. Larsson, P. Hansbo, K. Runesson, Strategies for goal-oriented a posteriori error measures in nonlinear elasticity, Int. J. Numer. Methods Engrg. 55 (2002) 879–894.
[20] L.Y. Li, P. Bettess, Notes on mesh optimal criteria in adaptive finite element computation, Commun. Numer. Methods Engrg. 11 (1995) 911–915.
[21] L.Y. Li, P. Bettess, J.W. Bull, T. Bond, I. Applegarth, Theoretical formulations for adaptive finite element computations, Commun. Numer. Methods Engrg. 11 (1995) 857–868.
[22] J. Mazars, G. Pijaudier-Cabot, Continuum damage theory – application to concrete, J. Engrg. Mech. 115 (1989) 345–365.
[23] J.T. Oden, S. Prudhomme, Goal-oriented error estimation and adaptivity for the finite element method, Comput. Math. Appl. 41 (2001) 735–756.
[24] E. Oñate, G. Bugeda, A study of mesh optimality criteria in adaptive finite element analysis, Engrg. Comput. 10 (1993) 307–321.
[25] T. Pannachet, H. Askes, L.J. Sluys, P-version error estimation for linear elasticity, Comput. Mech. 43 (2009) 603–615. doi: 10.1007/s00466-008-0333-8.
[26] B. Patzák, M. Jirásek, Adaptive resolution of localized damage in quasi-brittle materials, J. Engrg. Mech. 130 (2004) 720–732.
[27] R.H.J. Peerlings, Enhanced damage modelling for fracture and fatigue, Ph.D. Thesis, Eindhoven University of Technology, The Netherlands, 1999. <http://www.mate.tue.nl>.
[28] R.H.J. Peerlings, R. deBorst, W.A.M. Brekelmans, J.H.P. deVree, Gradient-enhanced damage for quasi-brittle materials, Int. J. Numer. Methods Engrg. 39 (1996) 3391–3403.
[29] G. Pijaudier-Cabot, Z.P. Bažant, Nonlocal damage theory, J. Engrg. Mech. 113 (1987) 1512–1533.
[30] S. Prudhomme, J.T. Oden, On goal-oriented error estimation for elliptic problems: application to the control of pointwise errors, Comput. Methods Appl. Mech. Engrg. 176 (1999) 313–331.
[31] R. Rannacher, F.T. Stuttmeier, A feed-back approach to error control in finite element methods: application to linear elasticity, Comput. Mech. 19 (1997) 434–446.
[32] R. Rannacher, F.T. Stuttmeier, A posteriori error control in finite element methods via duality techniques: application to perfect plasticity, Comput. Mech. 21 (1998) 123–133.
[33] R. Rannacher, F.T. Stuttmeier, A posteriori error estimation and mesh adaptation for finite element models in elasto-plasticity, Comput. Methods Appl. Mech. Engrg. 176 (1999) 333–361.
[34] A. Rodríguez-Ferran, A. Huerta, Error estimation and adaptivity for non-local damage models, Int. J. Solids Struct. 37 (2000) 7501–7528.
[35] K, Runesson, Strategies for goal-oriented a posteriori error measures in nonlinear elasticity, in: Proceedings of the15th Nordic Seminar on Computational Mechanics, Aalborg, Denmark, 2002. <http://www.ime.auc.dk/nscm15>.
[36] M. Rüter, E. Stein, Adaptive finite element analysis of crack propagation in elastic fracture mechanics based on averaging techniques, Comput. Mater. Sci. 31 (2004) 247–257.
[37] M. Rüter, E. Stein, F. Larsson, P. Hansbo, K. Runesson, Strategies for goal-oriented a posteriori error measures in nonlinear elasticity, in: Proceedings of the Second European Conference on Computational Mechanics (CDROM), Cracow, Poland, 2001.
[38] E. Schlangen, Fracture simulations of brittle heterogeneous materials, in: Proceedings of the 10th Conference Engineering Mechanics, ASCE, New York, 1995, pp. 130–133.
[39] A. Simone, Remarks on a gradient-enhanced damage model and its implementation, Studi e Ricerche 21 (2000) 243–282.
[40] A. Simone, H. Askes, R.H.J. Peerlings, L.J. Sluys, Interpolation requirements for implicit gradient-enhanced continuum damage models, Commun. Numer. Methods Engrg. 19 (2003) 563–572 (See also the corrigenda: Commun. Numer. Methods Engrg. 20, pp. 163–165).
[41] L.J. Sluys, M. Cauvern, R. deBorst, Discretization influence in strain-softening problems, Engrg. Comput. 12 (1995) 209–228.
[42] O.C. Zienkiewicz, J.Z. Zhu, A simple error estimator and adaptive procedure for practical engineering analysis, Int. J. Numer. Methods Engrg. 24 (1987) 337–357.